Title

Technologies for the Cryopreservation of 3D Bioprinted Scaffolds

Author

Warburton, Linnea

Publication Date

2024

Peer reviewed|Thesis/dissertation

Technologies for the Cryopreservation of 3D Bioprinted Scaffolds

By

Linnea Warburton

A thesis submitted in partial satisfaction of the

requirements for the degree of

Doctor of Philosophy

in

Engineering- Mechanical Engineering

in the

Graduate Division

of the

University of California, Berkeley

Committee in charge:

Professor Boris Rubinsky, Chair
Professor Grace O'Connell
Professor Costas Grigoropoulos

Spring 2024

Technologies for the Cryopreservation of 3D Bioprinted Scaffolds

By

Linnea Warburton

Abstract

Technologies for the Cryopreservation of 3D Bioprinted Scaffolds

by

Linnea Warburton

Doctor of Philosophy in Engineering- Mechanical Engineering

University of California, Berkeley

Professor Boris Rubinsky, Chair

The use of 3D bioprinted scaffolds has many advantages over the use of 2D cell culture for modeling the human body, as significant evidence shows that cells behave differently in 2D environments. Reliance on 2D cell culture during drug development contributes to high failure rate for new drugs. 3D bioprinted scaffolds are an alternative that can precisely mimic the 3D microenvironment of the body. However, the use of 3D bioprinting has been held back by the difficulty of cryopreserving 3D bioprinted scaffolds. Freezing a large, 3D scaffold creates an uneven temperature gradient and an unequal distribution of cryoprotectants, which compromises cell viability. This thesis presents "Temperature-Controlled-Cryoprinting" as a method of both fabricating and cryopreserving 3D bioprinted scaffolds. During Temperature-Controlled-Cryoprinting, a cell-laden ink is printed on a freezing plate. As each layer is printed, the print plate descends further into a cooling bath, which ensures that all cells in the scaffold are frozen at the same rate. In Chapter 2 of this thesis, we explore the fundamentals of Temperature-Controlled-Cryoprinting, including the impact that freezing has on the mechanical and material properties of the scaffolds. In Chapter 3, we discuss the optimization of the 3D printing process and how to enhance scaffold stability with crosslinking. In Chapter 4, we discuss the advantages of Temperature-Controlled-Cryoprinting for the cryopreservation of 3D bioprinted scaffolds. Finally, in Chapter 5, we conclude with a discussion about the ways in which Temperature-Controlled-Cryoprinting could accelerate drug development and offer future perspectives.

Table of Contents

List of Figures

List of Tables

Acknowledgements

I would first like to thank my PhD advisor, Dr. Boris Rubinsky, for all of his support and guidance throughout my PhD journey. I am immensely thankful for the opportunity to join the Rubinsky Biothermal lab at UC Berkeley, and I could not have had a better PhD experience. I learned so much from Dr. Rubinsky about how to be a better scientist, and what it means to be a part of the scientific community. Thank you to my qualifying exam committee, which included Dr. Lisa Pruitt, Dr. Grace O'Connell, Dr. Costas Grigoropoulos, and Dr. Kevin Healy. The questions and feedback I received during the qualifying exam helped guide my research for the remainder of my PhD. Thank you to all of my lab mates in the Rubinsky lab. Particularly, thanks to Leo Lou for his collaboration on the paper that became Chapter 2 of my thesis, and for all of his help and advice throughout my PhD. Thank you to Tony Consiglio, who was the senior student in the lab during my PhD and was always a source of knowledge. A big thank you goes to my wonderful friends, who were a constant source of joy during the past four years. In alphabetical order, I would like to thank Daniel, David, Emma, Erin, Gabby, Heya, Jake, Justin Kalloor, Justin Page, Katie, Li, Mackenzie, Matthias, Nayiri, Neerja, Numi, Sam, Stephanie, and Yertay. We had so much fun, and we have so much fun ahead of us!

Chapter 1

1. Introduction

1.1 Limitations of 2D Cell Culture

For over a hundred years, cell culture has been used for medical research, drug development, and the generation of biopharmaceuticals [1]. When grown in the laboratory, cells are typically cultured in a monolayer (one cell thick) on a vessel such as a petri dish and are covered in a liquid medium which delivers necessary nutrients. This technique is referred to as "2D cell culture," as the cells can spread only on one plane. 2D cell culture is used daily in laboratories across the world, as it is simple, efficient, and reproducible.

Beginning in the 1980's, however, researchers such as Mina Bissell began studying the impact of the extracellular matrix on cell behavior and found that cells cultured in 2D environment act differently than cells cultured in 3D environments such as the body [2]. Since then, researchers have demonstrated the following limitations for cells cultured in 2D. Cells cultured in 2D, 1) have an unusually flat, elongated shape, 2) Receive uniform amounts of nutrients from the cell media rather than variable amounts 3) have less cell junctions, 4) have less resistance to drugs, 5) proliferate at an unnaturally rapid pace, 6) have different gene and protein expression levels, and 7) respond differently to mechanical stimuli [3]. As a result, 2D cell culture is now considered an inaccurate representation of in vivo conditions.

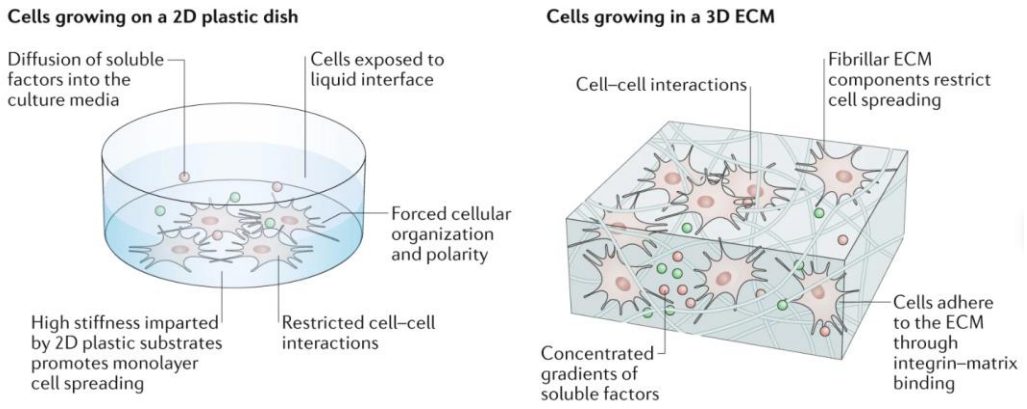

Figure 1.1 Cells grown in 2D are restricted to grow in a planar direction and to have apical-basal polarity. However, cells grown on a 3D extracellular matrix can attach in both planar and perpendicular directions and cell polarity is not restricted. Reprinted from Hussey et al. [4]

1.1.1 Reliance on 2D Cell Culture Impedes Drug Development

Drug development is a costly and lengthy process [5]. Developing and bringing a new drug to market can take up to 15 years, and cost between $800 million and $2 billion. Unfortunately, over 50% of drugs fail during the late stages of development [6]. The drug development process contains four stages, including phase I) drug discovery, phase II) preclinical development, phase III) clinical development, and phase IV) regulatory approval. 2D cell culture is still the most common choice for screening drug candidates, despite the known limitations [3]. For example, 2D cell culture is typically used to determine "ADMETox," which refers to a drug's absorption, distribution, metabolism, excretion and toxicity [5]. But 2D cell culture routinely produces false positives, which make drug candidates appear more promising than they actually are [7]. The physiological and physical properties of cells cultured in 2D makes them more susceptible to the effects of drugs than cells in 3D environments for several reasons. First, is due to a difference in the spatial arrangement and structure of surface receptors on the cell [3]. Since drugs often target particular receptors on the cell surface, these differences effect the binding efficacy of the drugs and produce different results. Second, cells cultured in 2D are typically all at the same cell stage, while cells cultured in 3D or in vivo are typically in different cell stages. This likely means that in 3D there are proliferating cells, and many drugs require proliferating cells to be effective. Finally, cells in 2D have a different shape than cells in 3D, which causes a difference in local pH within the cells. Researchers have demonstrated that lower intracellular pH levels reduce drug efficacy and contribute to drug resistance [3].

Despite promising results in initial stages with 2D cell culture, drug development must often be terminated later due to lack of drug efficacy or due to toxicity [6]. Therefore, one of the main areas that could improve drug success rate would be replacing the use of 2D cell culture with more advanced models. Reducing the drug failure rate would hasten medical innovation and improve the lives of countless patients.

1.2 3D Cell Culture as an Advanced Method

An alternative to the use of 2D cell culture is to culture cells in *in vitro* 3D environments. When cultured in 3D, the following advantages are present. 1) The natural cell shape is preserved, 2) a nutrient gradient can be created 3) cell-to-cell communication is allowed through cell junctions 4) proliferation rates are more realistic 5) protein and gene expression levels are similar to in vivo levels 5) cells respond accurately to mechanical stimuli [3]. The complexity of 3D cell culture

methods varies, with higher complexity models becoming a more accurate model of *in vivo* tissue. Ideally, the 3D model should simulate a specific tissue, and include the specific microenvironment of that tissue. For example, the model should include tissue-specific stiffness, nutrient gradients, oxygen gradients, metabolic waste gradients, and scaffolding cells [2].

The simplest form of 3D cell culture is the creation of "spheroids," which refer to cell aggregates which self-organize into a sphere during cell proliferation (See Figure 1.2.). These cell aggregates can be formed in environments that prevent the cells from attaching to a flat surface, such as hanging drop culture or encapsulation in a hydrogel [8]. "Organoids" are similar to "Spheroids" but with an increased level of complexity. Organoids are spherical, self-organizing aggregates that may contain multiple cell types and are typically intended to model particular tissues and organs [2].

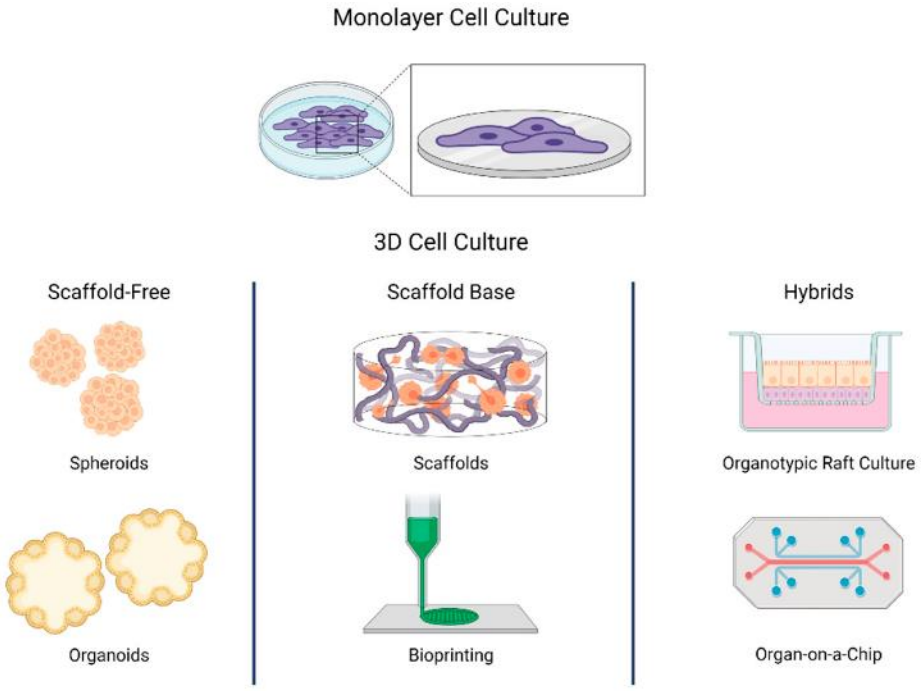

Figure 1.2 Types of 3D cell culture. Reprinted from de Dios-Figueroa [9]

One of the limitations of spheroids and organoids is the lack of organ level structures and tissue-tissue interfaces [3]. This limitation has been addressed by the development of "Organ-on-a-Chip" systems, which are microfluidic chips populated with living cells. "Organ-on-a-Chip" systems can be used to create organ-level structures that function like *in vivo* organs. They also allow for high resolution and real-time imaging which makes it easy to analyze the metabolic, genetic, and biochemical activities that are difficult to analyze in *in vivo* tissue [3].

A final technique for fabricating 3D cell culture is 3D bioprinting, which is the focus of this thesis. 3D bioprinting refers to the use of 3D printing to fabricate cell-laden scaffolds. The invention of this technology is considered a significant advancement for the tissue engineering field. 3D bioprinting can be used to fabricate multi-material scaffolds with the precise placement of multiple cell types, which allows researchers to closely mimic native tissue design [10]. Each of the 3D cell culture methods mentioned here has its unique advantages, and 3D bioprinting is particularly advantageous for the ability to create intricate geometries, and to do so in a repeatable manner. Most of the advanced methods of 3D cell culture have been developed in the past twenty years. "Organ-on-a-chip" systems, which are micro, biomimetic platforms, were invented in the early 2000's, and the use of organoids, aka 3D masses of self-organized 3D tissue, became common starting in the 2010's, [11,12]. 3D bioprinting became popular in the early 2000's as well [13]. Since then, interest in 3D cell culture has grown significantly.

Furthermore, in 2022, the United States passed the FDA Modernization Act 2.0, which enables the use of cell-based assays to investigate the safety and efficacy of a drug, rather than animal testing [14]. The FDA Modernization Act has created an urgent demand for repeatable 3D cell culture methods to be used in clinical trials and reaffirms the immense potential of this technology. The replacement of 2D cell culture by 3D cell culture methods could revolutionize medical research, drug development, and biopharmaceutical production.

1.3 Introduction to 3D Bioprinting

"3D Bioprinting," to put it simply, refers to the use of 3D printing to fabricate cell-laden scaffolds. There are many types of 3D bioprinting, from inkjet, to laser-assisted, to extrusion bioprinting [14]. Extrusion based bioprinting is the most common and low-cost option, and it will be the focus of this thesis. Before the start of the bioprinting process, cells are mixed into a viscous material to form a "bioink." Typically, the viscous material is a hydrogel, which is a polymer-based material which holds a large amount of water. Ideally, the bioink should have similar biological properties to the target tissues, such as cell-binding sites that allow for cell attachment, growth, spreading, and differentiation [15]. Some common bioinks include collagen, alginate, gelatin methacrylate (GelMA), or hyaluronic acid.

In addition, the bioink should have mechanical and rheological properties that allow it to be extruded through the nozzle during 3D printing and maintain its shape. A notable challenge during 3D bioprinting is that the bioinks must be soft, and low viscosity in order to be extruded through the nozzle. But once they are extruded, it may be difficult for these soft materials to hold their printed shape. Therefore, most 3D bioprinting processes must also contain a "crosslinking" step to stiffen the printed structure. "Crosslinking" refers to the formation of bonds between the polymer chains of a material, and it turns a low viscosity material into a stiffer gel. Based on the bioink, there are various crosslinking options such as thermal crosslinking, photocrosslinking with UV light, or ionic crosslinking by adding oppositely charged ions (See Table 1.1) [16-18].

Table 1.1 Crosslinking Strategies for 3D Bioprinting

Type of Crosslinking	**Common Materials**	**Notes**	**Notable Examples**
Ionic Crosslinking Using metal ions	Sodium Alginate + $CaCl_2$	• Most commonly used type of crosslinking • Crosslinking agent can be added during printing or after • Can be extruded with a second nozzle, added in a support bath, aerosolized, etc • Can be coupled with thermal gelation during printing and ionic crosslinking after printing has finished • The metal ions may damage cells if concentration is too high	Ahn et al., Cell viability of ~84% [19]
Without metal ions		• Uses electrostatic bonding of ionically charged hydrogels • Opposite charged hydrogels for electrostatic bonds • Reversible, may not improve the mechanical stability of the print enough alone • Usually used with second crosslinking process	Li et al used anionic and cationic inks, Cell viability of ~96% [20]
Non-Covalent Crosslinking	• Silk-based bioinks	• Reversible, thus prints may have poor mechanical stability if this crosslinking strategy is used alone	Wang et al., used silk-based bioink [21]

• Ph or β-sheet crystallization		• A promising option as cell viability may be impacted less than other crosslinking methods	
Thermal Crosslinking	Sodium Alginate Various forms/concentrations of Agarose, which forms a gel under ~32 °C MC (Methylcellulose) bioinks, viscous solution at room temp, gels at ~37°C (reversible) Collagen	• Reversible, and thus often used in conjunction with a second crosslinking method • Thermal crosslinking at temperatures between 0°C and 40°C is time intensive, for example Agarose hydrogels may take 30 minutes to fully gel	Use of cryogenic temperatures, such as by Ukpai et al, or Tan et al. [21-23] Daly et al. cooled Agarose under 32°C until it formed a gel [24]
Photo Crosslinking • Extrusion-based • Stereolithography • Digital light processing • Laser-assisted methods • Volumetric bioprinting	• Bioink: GelMa is most • commonly used • Photoiniators: Irgacure 2959 and lithium-acyl phosphinate (LAP) are most commonly used	• Use of Photocurable bioink + photoinitiators • Can use UV light or visible light, but repeated use of UV light damages cells • High print speed • Support structures may not be needed • Limits material choice, as bioink must be photocurable	Kelly et al. used Computed Axial Lithography to print soft GelMa structures [25] Na. et al., fibroblast cell viability of ~90% [26]

Enzymatic Crosslinking	Enzymes used: • trans-glutaminase, •phosphopantetheinyl transferase, • lysyl oxidase, • plasma amine oxidase • peroxidases horseradish peroxidase mimetic enzymes.	• Enzymatic reactions are relatively mild, so this is a promising method for reducing cell death from crosslinking • Usually used in combination with other crosslinking methods as alone it may not offer enough mechanical stability by itself. Often enzymatic crosslinking is used first and then ionic or photo crosslinking is used after.	Zhou et al. GelMa hydrogel, enzymatic crosslinking with microbial transglutaminase [27] Shi et al. GelMa + collagen bioink that was enzymatically crosslinked with tyrosinase, later photo crosslinked as well (Cell Viability of ~90%) [28] Costa et al. used silk-based hydrogel , enzymatically crosslinked with horseradish peroxidase (HRP) [29]

Therefore, a typical process of extrusion 3D bioprinting is as follows. First, cells are mixed into a viscous material to form a bioink. Second, the bioink is extruded through the nozzle onto the print plate in a particular shape. Third, a crosslinking step is performed to improve the mechanical properties of the 3D printed scaffold. Fourth, cell media is added to the cell-laden scaffold, which is then cultured in the incubator for days or weeks.

3D bioprinting is a promising technology, because it allows unprecedented control over the architecture of the scaffold and the placement of various cell types [30,15]. This technology has several other unique advantages [30]. First, 3D bioprinting has high reproducibility compared to previous methods used to generate scaffolds, such as freeze-drying or particulate leaching. Second, 3D bioprinting allows for the fabrication of scaffolds using medical imaging such as computed tomography (CT) or magnetic resonance imaging (MRI). Third, 3D bioprinting can be used to

fabricate scaffolds with multiple materials and multiple cell types, and the placement of each cell type within the scaffold can be carefully controlled. Fourth, 3D bioprinting can be used for the controlled delivery of growth factors and drugs. Fifth, 3D bioprinting can create vascular structures within tissues, expanding the size of engineered tissues.

1.3.1 3D Bioprinting for Drug Development

Within the context of drug development, 3D bioprinting poses advantages for drug screening, drug delivery, ADME assays, and high-throughput drug testing [30]. During drug discovery, 2D assays are used to screen leading drug candidates, and 2D assays are used to exclude candidates with unacceptable toxicity levels. As discussed previously, these 2D assays are highly inaccurate, both exaggerating the efficacy of drug candidates and failing to predict toxicity in later stages. Replacing these steps with a 3D bioprinted scaffold that better mimics in vivo tissue would save valuable time and resources during drug development. Several studies have used 3D bioprinted scaffolds produced with low to high-throughput manufacturing to explore their potential as in vitro models for drug efficacy and drug toxicity, though few scaffolds have been commercially implemented. One notable success is the "exVive3D" liver tissue model developed by Organovo to screen for liver toxicity. The 3D bioprinted liver model included hepatocytes, endothelial cells, and stellate cells in a hexagonal unit. The liver model produced liver proteins including fibrinogen and albumin for longer than 42 days. Two drugs were tested on the liver model, Levofloxacin, a commercially available and therefore "safe" drug, and Trovafloxacin, a failed drug candidate. Trovafloxacin had been found safe using 2D assays during the pre-clinical stage, but then later failed in phase III because of liver toxicity. Organovo's liver models demonstrated safety for Levofloxacin, the commercially available drug, and demonstrated toxicity for the failed drug [30]. The "exVive3D" liver model is a clear example of how the use of 3D bioprinted scaffolds could accelerate the drug development process. Another notable success has been demonstrated with the use of 3D bioprinted scaffolds for screening chemotherapy (anti-cancer) drugs. Sun et al 3D bioprinted a *in vitro* cervical tumor model, and found that the 3D bioprinted scaffolds were more chemoresistant to Paclitaxel than 2D cell assays [31].

3D bioprinting offers unique advantages for high-throughput drug screening, due to the automated nature of this fabrication method. Previously, several groups have demonstrated the ability of 3D bioprinting to create high-throughput arrays. Rodríguez-Dévora et al used an inkjet printer to create a miniature, high-throughput drug screening platform [32]. Xu et al developed an automated, high-throughput bioprinting system that could produce a 3D model containing fibroblasts and cancer cells [33].

Finally, 3D bioprinted models could be used to analyze "ADME" aka absorption, distribution, metabolism, and excretion of drugs. These ADME properties determine the way that drugs are administered and metabolize in the body, and they are typically analyzed during the preclinical phase. Typically, 2D assays and animal models are used to analyze ADME properties, and due to the FDA modernization act, both of these steps could potentially be improved by the

use of 3D bioprinted scaffolds. Previously, Chang et al used 3D bioprinted micro-livers to analyze drug metabolism [34]. In summary, there are many promising examples of 3D bioprinted scaffolds being used for drug development, though few systems have been scaled up for commercial use.

1.4 Current State of Cryopreservation of 3D bioprinted Scaffolds

Despite the promising applications of 3D bioprinting, this technology has been slowly adopted as an alternative for 2D cell culture. While 2D cell culture is simple and efficient to use, 3D bioprinting is time-consuming, and requires additional devices and trained personnel. Currently, 3D bioprinting lacks high throughput methods which would allow it to become as ubiquitous as 2D cell culture. A major obstacle is the difficulty in cryopreserving 3D cell culture [35]. Cryopreservation is a fundamental tool that underpins the use of biological material. Cells are routinely frozen for both short-term (weeks) to long-term (years) storage. If not for the use of this "biological pause," continuous cell lines would experience genetic changes and finite cell lines would experience aging and transformation. When cells are transported from laboratory to laboratory, they are commonly done so in a cryopreserved state so that the cells can survive the journey. For laboratories using cells, cryopreservation is both a regular and necessary occurrence.

If 3D bioprinted scaffolds could be effectively cryopreserved, they could be manufactured in a specialized 3D bioprinting lab and then shipped to other labs. The ability to store 3D bioprinted scaffolds on a short-term or long-term basis would make it possible to manufacture a higher number of them and then use them for high throughput screening. Access to 3D cell culture as a shelf-stable, ready-to-use, standardized product would greatly accelerate adoption of this technology [36, 37]. Therefore, in order for 3D bioprinted scaffolds to achieve their full potential, there must be effective methods of cryopreserving them [36, 35].

1.5 Cell Death during Cryopreservation

Cryopreservation of biological material typically involves the following steps [39].

1. Addition of cryoprotective agents (CPAs) to the cells before cooling begins.
2. Cool the cells down to a low temperature, such as -196°C.
3. Rewarm the cells.
4. Remove the CPAs from the cells after thawing.

Cells face severe chemical and physical stresses during this process, which often leads to death [38]. One common misconception is to believe that the lower the temperature, the more damage should occur to the cell. In fact, it is not storage at low temperatures such as -196°C in

liquid nitrogen that is most lethal to cells [39]. Instead, the most dangerous temperatures for cells lie between -15°C to -60°C. During freezing down to -196°C, and then being thawed back up to room temperature, cells must traverse this “danger zone” twice, and it is here that the most cell damage occurs.

During cryopreservation, stresses to cells include 1) cold stress 2) extracellular or intracellular ice formation, and 3) osmotic stress during cryoprotectant addition and removal, and 4) chemical toxicity of some cryoprotectants. Cryopreservation-induced cell death manifests for about 24 hours post-thaw, and therefore cell viability tests done during cryopreservation studies should take place at least 24 hours after thawing. These stresses cause cell death in the following ways. Cold stress alters the lipid composition of the cell membrane, which can cause cell leakage, and also reduces the rate of protein synthesis and cell proliferation [40]. Extracellular ice formation increases the solute concentration around the cells, which creates osmotic pressure which draws water out of the cells. This alters the intracellular solute concentration and pH, which can be toxic. In addition, excessive cell shrinkage from cell dehydration can also be physically damaging to internal structures [41]. During intracellular ice formation, the sharp ice crystals can rupture the cell membrane, which later leads to cell death when the cells thaw.

To reduce cell death from ice formation, cryoprotectants can be added to the cells before cryopreservation. Some common cryoprotectants include DMSO, glycerol, trehalose, and disaccharides. There are two classes of cryoprotectants, those that are permeable to the cell, or those that are non-permeable. Permeable cryoprotectants typically permeate the cell membrane and reduce intracellular ice formation as well as osmotic shrinkage. Non-permeating cryoprotectants, which are often sugars, augment the use of a permeable cryoprotectant and are rarely used without a permeable cryoprotectant [39]. Using a non-permeable cryoprotectant can reduce extra cellular ice formation and can stabilize the cell membrane.

1.5.1 The Importance of Freezing Rate

The use of particular freezing rates is crucial to the survival of cells during cryopreservation. If cells are cooled too slowly during cryopreservation, their volume will shrink significantly, and they will be exposed to too high levels of solutes concentrations (See Figure 1.3). But if cells are cool too quickly, large ice crystals form that rupture the cell membrane. Therefore, there are two established freezing rates that are used to cryopreserve cells. The first is slow freezing, at around 1°C/min, and the second is vitrification at around 10^6 °C/min. During vitrification, the solution surrounding the cells transforms from a liquid to a glassy state and ice formation does not occur. Slow freezing and vitrification each have their own benefits and limitations. This thesis will focus on the use of slow freezing to cryopreserve 3D bioprinted scaffolds, as it is applicable for a wide range of cell types and it is easier to develop cryopreservation technology that does not require the high freezing rates of vitrification.

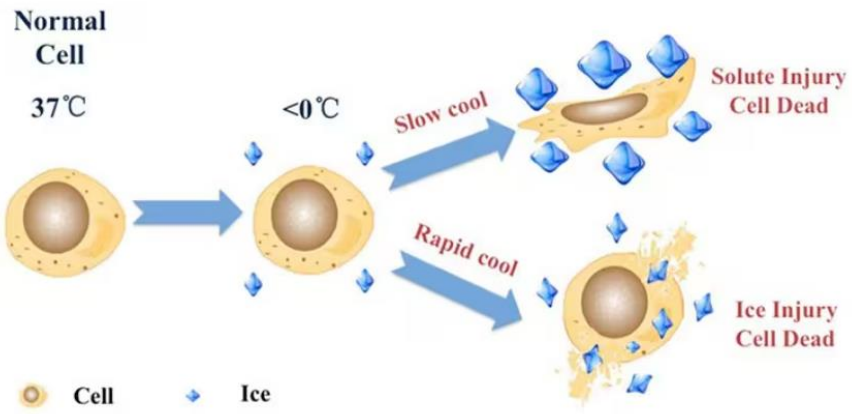

Figure 1.3 Cooling too slowly or too rapidly results in cell death during cryopreservation. Figure reprinted from ECACC Handbook Fundamental Techniques in Cell Culture Laboratory Handbook – 4th Edition [42]

1.6 "Temperature-Controlled-Cryoprinting" as a Promising Cryopreservation Method

Unfortunately, the established methods for cryopreserving cells in 2D are not effective for cells in 3D environments. When expanding from 2D to 3D, there are two issues that prevent successful cryopreservation (See Figure 1.4). The first is a heat transfer issue, and the second is a mass transfer issue regarding the diffusion of cryoprotectants. Regarding the heat transfer issue, freezing from outside inward creates an uneven temperature gradient throughout the scaffold such that the cells are frozen at different rates. As discussed previously, the rate at which cells are frozen is crucial for cell survival. The second issue is the non-uniform distribution of cryoprotectants. When cryoprotectants are introduced from the exterior of the object, cells deep in the scaffold risk being exposed to insufficient levels of cryoprotectant, and cells at the surface of the scaffold risk death from cryoprotectant toxicity. Both of these issues become magnified the larger the size of the scaffold. Although there have been some successes in cryopreserving tissue-engineered scaffolds, cell viability was often below 50% and the size of the scaffolds was often less than 0.15 cm^3 [35].

Figure 1.4 The cryopreservation of 3D objects is challenging due to first, difficulty of distributing cryoprotectant uniformly throughout the object and second, achieving a uniform freezing rate throughout the object.

Rather than freezing a completed 3D bioprinted scaffold, a more promising approach is to combine the two steps of 3D printing and cryopreservation into one step. This approach for cryopreserving tissue-engineered scaffolds was invented by Adamkiewicz et al in 2008 and named 3D cryoprinting [43] During 3D cryoprinting, the bioink is extruded through a nozzle onto a freezing plate. In addition to cryopreservation, the use of 3D cryoprinting has several benefits within the field of tissue engineering. First, freezing the object as it is 3D printed increases its rigidity, facilitating the manufacturing of complex structures from an ink that is usually soft at deposition [23,44]. Second, freezing cell-laden bioinks at optimal cooling rates during deposition can preserve the cells, preventing them from succumbing to environmental stressors during the printing process. Third, by combining 3D printing and freezing into one step, the manufacturing process is streamlined, which enables this technology to be scaled up for mass manufacturing of 3D bioprinted scaffolds.

Few researchers have attempted to use 3D cryoprinting to cryopreserve cell-laden scaffolds. In 2020, Lee et al used a microfluidic printing device to cryopreserve preosteoblasts (MC3TC-E1) [45] The microfluidic nozzle had a core and a outer shell region. The shell region was composed of GelMA, alginate, and DMSO, while the core region was filled with collagen, DMSO, and cells in media. After printing onto a freezing plate at a variety of temperatures, the scaffold was frozen at 1°C/min down to -80°C and cryopreserved overnight. The scaffold was then thawed for 10 minutes in 37C media and crosslinked with UV light. The highest scaffold printed during this study was 3 layers tall, and the maximum cell viability was 85%. They optimized the temperature of the freezing plate, core region, and shell region to maximize cell viability. The freezing plate was set at either -20°C, -15°C, -10°C, or -5°C. The core region was set at either 25°C, 10°C, or -5°C. And the shell region was set at either 25°C, 15C, or 5C. The highest viability was achieved at a plate temperature of -5°C, a core temperature of -5°C, and a shell temperature of 5°C. With these temperatures, the cooling rate of the cells in the bioink as it was extruded onto the freezing plate was the slowest, which is in line with the theory of slow cooling. In addition to

the temperature conditions, Lee et al also optimized the GelMA concentration, flow rate, and UV intensity to maximize cell viability and printability.

In 2021, a paper by Luo et al used cryoprinting to print cell-laden bioink in the vertical direction [46]. Unlike other 3D bioprinting methods, the use of a freezing plate allowed the soft bioink to freeze and stabilize, allowing freestanding filaments to be printed. The filaments had anisotropic, interconnected pores as a result of the directional formation of ice crystals up the z-axis during freezing. These pores were ideal for anisotropic cell growth within the scaffold, and also enhanced mechanical performance. Luo et al investigated the use of skeletal myoblasts in these filaments, and found enhanced spreading and alignment compared to filaments that were not directionally frozen. This technique has applications in interface issue engineering, for example the creation of a muscle-tendon unit. During this study, DMSO was used in conjunction with melezitose as cryoprotectants, and GelMA was used as the bioink.

Later in 2021, a paper by Ravanbakhsh et al from the same group explored a similar technique they named "cryobioprinting" [47]. They modified a 3D bioprinter with a freezing plate and extruded a cell-laden GelMA bioink onto it. The GelMA scaffold was then cryopreserved down to -80C and crosslinked with UV light during thawing. Ravanbakhsh explored the use of various cryoprotectant compositions, including various concentrations of DMSO, and the use of six saccharides such as trehalose, lactose, sucrose, raffinose, melezitoze, and maltose. Their results suggested that 10% DMSO was the optimal concentration and that 12% (w/v) melezitose was the highest performing disaccharide in conjunction with DMSO. They printed a range of 2D and 3D structures with the optimized bioink to confirm the printability of the chosen bioink. Then, they used a bioink laden with human mesenchymal stem cells for cryobioprinting, and demonstrated their chondrogenic, osteogenic, and adipogenic differentiations. They also assessed the angiogenesis potential of the cryopreserved scaffolds with a chorioallantoic membrane (CAM) assay and found vascular growth and vessel formation. They stored their cryopreserved scaffolds for up to 3 months without a reduction of cell viability. Ravanbakhsh noted that one limitation of their study was that printing above a certain thickness resulted in the top layers of the scaffold no longer freezing, which limited the size of the scaffolds.

These approaches can be classified as "static" cryoprinting, as they involve printing onto a static freezing plate. A notable limitation of static cryoprinting is that as each layer is printed, the last printed layer moves further away from the freezing plate and so the temperature of the last printed layer rises. As noted by Ravanbakhsh et al., 2022, the reduced heat transfer rate as printing continues prevents the printing of thick constructs and leads to cell death in the higher layers [37].

As an advancement to this field, this thesis presents "Temperature-Controlled-Cryoprinting" as a novel method of cryopreserving 3D bioprinted scaffolds. The technology is based on the method derived from Adamkiewicz et al, which uses a dynamic freezing plate to avoid the limitations associated with static cryoprinting. During Temperature-Controlled-Cryoprinting, a cell-laden bioink is printed onto a freezing plate. As each layer is printed, the print plate descends further into the cooling bath by the height of the layer. As a result, the lower layers of the printed scaffold become immersed in the cooling fluid and the temperature at the nozzle is kept constant. Unlike static cryoprinting, there is no height limit, as the new layers will continue to freeze and the earlier layers will continue to cool as they descend further and further into the cooling bath.

1.7 Thesis Overview

As the use of 3D cell culture becomes more desired, there is an urgent need to develop cryopreservation approaches. The use of "3D cryoprinting," which combines 3D bioprinting and cryopreservation into one step is a promising approach that could address the heat transfer and mass transfer issues that occur when cryopreserving thick, 3D scaffolds. This thesis develops "Temperature-Controlled-Cryoprinting" as a method of cryopreserving 3D bioprinted scaffolds. Chapter 2 explores the fundamentals of Temperature-Controlled-Cryoprinting and addresses the following questions. First, how does freezing affect the mechanical properties of the 3D bioprinted scaffold? Second, is it possible to change the size and shape of pores in the scaffold created by ice crystal formation by changing the freezing rate? Third, how will crosslinking before or after freezing impact the mechanical properties and structure of the scaffolds? Chapter 2 investigates the influence of crosslinking order and cooling rate on the microstructure and mechanical properties of single-layer, sodium alginate scaffolds. We designed and built a novel modular 3D printer in order to study the effects of these steps separately and to address many of the manufacturing issues associated with 3D cryoprinting. With the modular 3D printer, 3D printing, crosslinking, and freezing were conducted on separate modules yet remain part of a continuous manufacturing process. Crosslinking before the freezing step produced highly interconnected and directional pores, which are ideal for promoting cell growth. By controlling the cooling rate, it was possible to produce pores with diameters from a range of 5 μm to 40 μm. Tensile and firmness testing found that the use of freezing does not decrease the tensile strength of the printed objects, though there was a significant loss in firmness for strands with larger pores.

The modular 3D cryoprinter was developed for exploring the fundamentals of cryoprinting, by studying each step separately. But a novel device was required in order to combine these steps and print multi-layer scaffolds. Chapter 3 presents the design of a novel, Temperature-Controlled-Cryoprinter which has the ability to print multi-layer structures under uniform thermal conditions. Despite the ability to print multi-layer scaffolds out of soft bioinks, crosslinking the frozen objects before they thawed and collapsed remained a challenge. In Chapter 3, we developed a process for crosslinking frozen objects which we name "freezing-modulated-crosslinking." [48]. After 3D cryoprinting is complete, the frozen object can be stored in a freezer for short-term or long-term use. Then, when the scaffold is ready to be used, freezing-modulated-crosslinking is used to thaw the frozen object at a controlled rate inside a bath of crosslinker such that it maintains its initial shape. Finally, the scaffold can be used for tissue-engineering applications. The challenge is to control the thawing rate of the frozen object, so that the rigidity provided by freezing is replaced by cross linking as the Ca+ ions diffuse into the thawed region. Crosslinking alginate structures in a bath of $CaCl_2$ is a common crosslinking technique used in 3D bioprinting. However, to the best of our knowledge, this is the first time that temperature control of the $CaCl_2$ bath has been used to crosslink layer-by-layer in order to maintain the structure of a soft printed object. In addition, this

is the first time the parameters of freezing-modulated-crosslinking have been investigated in order to optimize the structure of the printed object.

The development of Freezing-Modulated-Crosslinking required two parts, a mathematical analysis, and an experimental validation. In part 3.3, a dimensionless analysis was used to determine what and how the thermal parameters control the process of freezing-modulated-crosslinking. Our mathematical analysis finds that two temperature parameters can be used to control the process: the surface temperature of the melting object and the initial temperature of the frozen sample. In Part 3.4, we qualitatively examine the effect of these parameters by printing various shapes out of 2% sodium alginate and crosslinking them in a $CaCl_2$ bath with freezing-modulated-crosslinking. To further characterize freezing-modulated-crosslinking, we also examine the impact of $CaCl_2$ concentration. The results demonstrate the feasibility of this technique and qualitatively confirm the predictions of the mathematical model. Freezing-modulated-crosslinking can therefore be used to crosslink frozen scaffolds printed out of soft bioinks without the objects losing their intended shape. An object temperature of -80°C, and a crosslinker bath temperature of -0.05°C produced objects that most closely resembled the intended results. The concentration of $CaCl_2$ in the crosslinker bath did not have a statistically significant impact on the size or shape of the objects. The development of freezing-modulated-crosslinking expands the type of biomaterials that can be used for 3D cryoprinting and the type of structures that can be printed out of soft bioinks.

Chapter 2 and Chapter 3 explored the fundamentals of cryoprinting and developed methods for printing multi-layer scaffolds and crosslinking them. However, this technology had only been used with a-cellular versus cell-laden scaffolds. Chapter 4 assesses the efficacy of using Temperature-Controlled-Cryoprinting to cryopreserve cell-laden hydrogels. The Temperature-Controlled-Cryoprinter described in Chapter 3 was used to print Vero cells encapsulated in an alginate-collagen bioink [105]. The freezing-modulated-crosslinking process developed in Chapter 3 was used to crosslink the alginate-collagen scaffolds with $CaCl_2$ during thawing.

The purpose of Chapter 4 was to maximize cell viability during Temperature-Controlled-Cryoprinting. Experiments were done to identify which stages of the cryoprinting process resulted cell death, and parameters were adjusted to reduce cell death. We developed an optimal temperature profile for freezing during 3D printing and evaluated drops in cell viability during the various stages of Temperature-Controlled-Cryoprinting. Chapter 4 found that Vero cells in an alginate-collagen bioink can survive Temperature-Controlled-Cryoprinting and cryopreservation at -80°C with a viability of 71.64% ± 7.47 in multi-layer scaffolds. Printing with an initial bioink temperature of 0°C onto a printing plate at -5°C resulted in a higher cell viability than using a bioink temperature of 4°C or 25°C, and our experiments suggested that this was due to the slower cooling rate during printing. Surprisingly, cell exposure to DMSO during Temperature-Controlled-Cryoprinting did not pose an issue. Most notably, Temperature-Controlled-Cryoprinting was used in this study to print an eight-layer scaffold, which was higher than has been achieved with static cryoprinting. Experiments showed that cell death did not increase as higher layers were printed but remained constant throughout the scaffold. Temperature-controlled cryoprinting thus solves an important limitation of static cryoprinting, which is that the cooling rate decreases as further layers are printed and become further away from the print plate.

In summary, this thesis explored the use of Temperature-Controlled-Cryoprinting for the cryopreservation of 3D bioprinted scaffolds. Chapter 2 demonstrated that including freezing in the

3D bioprinting process did not damage the mechanical properties of the scaffolds, and in Chapter 3, new technologies were developed for the cryoprinting and crosslinking of multi-layer scaffolds. In Chapter 4, this technology was then utilized for cryopreserving cell-laden scaffolds and modified to optimize cell survival. Temperature-Controlled-Cryoprinting was found to be an effective method of cryopreserving 3D bioprinted scaffolds that resulted in higher cell viabilities than reported by the literature, and the highest number of layers in a cryopreserved 3D bioprinted scaffold to date.

Chapter 2

2. Fundamentals of 3D Cryoprinting

2.1 Introduction

Chapter 2 investigates the influence of crosslinking order and cooling rate on the microstructure and mechanical properties of single-layer, sodium alginate scaffolds. When used with alginate bioinks, this type of 3D cryoprinting requires three steps: 3D printing, crosslinking, and freezing. This study investigated the influence of crosslinking order and cooling rate on the microstructure and mechanical properties of sodium alginate scaffolds. We designed and built a novel modular 3D printer in order to study the effects of these steps separately and to address many of the manufacturing issues associated with 3D cryoprinting. With the modular 3D printer, 3D printing, crosslinking, and freezing were conducted on separate modules yet remain part of a continuous manufacturing process. Crosslinking before the freezing step produced highly interconnected and directional pores, which are ideal for promoting cell growth. By controlling the cooling rate, it was possible to produce pores with diameters from a range of 5 μm to 40 μm. Tensile and firmness testing found that the use of freezing does not decrease the tensile strength of the printed objects, though there was a significant loss in firmness for strands with larger pores.

One of the potential advantages of freezing during printing is that microscale pores are created by the ice crystal growth in the printed object. Tissue-engineered scaffolds must be highly porous for cell seeding and ingrowth, with typical porosities above 90% [49]. In fact, 3D bioprinting is often chosen as a fabrication method for tissue-engineered scaffolds because of its ability to precisely print macropores on the scale of 1mm. Thus, 3D bioprinting coupled with freezing can be used to create complex structures with both controlled macropores and micropores for cell growth. In the various methods of 3D cryoprinting, the process of freezing occurs along the temperature gradient, on a specific axis. When freezing occurs along a specified axis, this process is known as directional freezing. During directional freezing, ice crystals grow forward as a dendritic ice front, creating directional pores (See Figure 2.1).

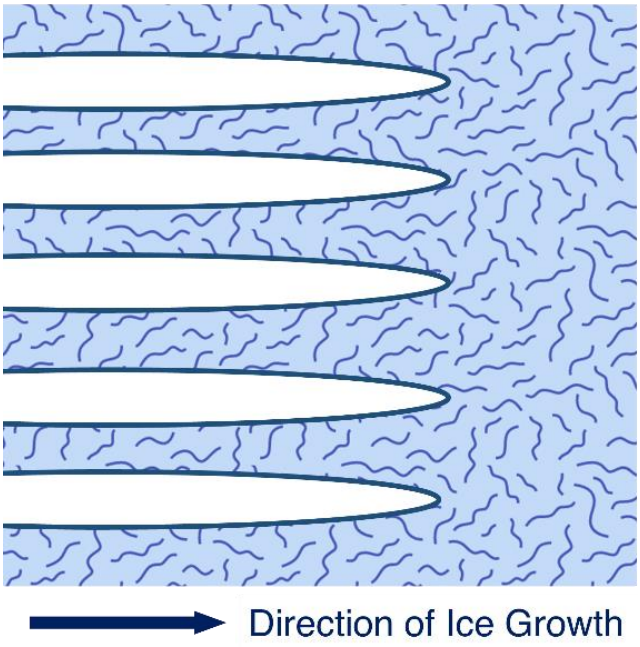

Figure 2.1 Ice crystal growth along an axis during directional freezing

This directionality has special significance within the field of tissue engineering, as directional, interconnected pore networks within scaffolds are crucial for cell growth [50]. An interconnected pore network encourages cell attachment and vascularization, while directional pores aid directional cell growth and provide faster diffusion for drug delivery. [51-52]. While directional freezing has rarely been studied in conjunction with 3D bioprinting, it has been used extensively to create directional, interconnected pores in biomaterials [51, 53-57] 12-16, 9]. Notably, Bozkurt et al used directional freezing to create longitudinal pores in collagen scaffolds for axonal regeneration, and Qi et al used directional freezing to create oriented pores in alginate/calcium phosphate cement (CPC) scaffolds [58-59].

Chapter 2 will address several important manufacturing issues related to 3D cryoprinting, with a focus on cryoprinting with alginates. Alginates are one of the most popular materials used as bioinks [60,16]. In order for a bioink to be considered for 3D bioprinting, it must be biocompatible, extrudable though the nozzle, and able to withstand its own weight to maintain the shape of the 3D printed scaffold. Alginate is a common choice because of its excellent biocompatibility, and its ability to promote wound healing [16]. In addition, alginate can be crosslinked with ionic crosslinking, and is commonly crosslinked with calcium ions. This allows the alginate to be extruded through the nozzle and then crosslinked to hold the shape of the printed object. Crosslinking the alginate before printing results in an ink with a variable viscosity that increases in time – causing difficulties in designing the ink flow through the printing nozzle. Therefore, the alginates are often crosslinked during or after the deposition of the printed material. Another key advantage of alginate is its tunable mechanical properties [62]. By changing the

concentration of alginate or the crosslinking density, it is possible to control the stiffness of the 3D bioprinted scaffold.

In 3D cryoprinting, there is another manufacturing step in addition to printing and crosslinking, which is freezing. Therefore, the order of manufacturing the 3D cryoprinted object can be either: a) deposition, freezing, thawing and crosslinking or b) deposition, crosslinking, freezing and thawing. A major goal of the freezing process in cryoprinting is to generate controlled microstructures with desired dimensions and orientation. This can be achieved through controlled cooling rates during freezing. Another important question in the design of a manufacturing process using cryoprinting is how does the freezing and the resulting microstructure affect the ultimate mechanical properties of the printed object. Porous hydrogels for tissue engineering must have high porosity while maintaining mechanical strength, or they will not survive in the body [63]. The goal of this experimental study is to evaluate how the parameters of a typical 3D cryoprinting process, including cooling rate and order of crosslinking, affect the microstructure and the mechanical properties of a 3D printed object. To study the effect of each step separately, we have designed a modular 3D printer in which the steps of printing, freezing and crosslinking are done separately in the desired order and with the desired parameters. To facilitate breaking apart these three steps, while maintaining continuity of the manufacturing process, each step takes place on a moving stage that allows the printed object to move from one module to another. In addition to serving as a means for fundamental studies, this modular technology may also have value as an industrial means for large scale continuous manufacturing of bioengineering products.

Using the modular 3D printer, we investigate the influence of crosslinking and cooling rates over the shape and distribution of the pores within 3D printed sodium alginate strands. The first goal of this study was to investigate how crosslinking before or after directional freezing impacts the creation of pores. The second goal was to investigate the influence of cooling rate on the shape and size of the pores. The third goal was the evaluate whether the use of directional freezing negatively affected the mechanical properties of the sodium alginate scaffold. The tensile strength and firmness of each type of directionally frozen scaffold was tested to evaluate if the directionally frozen scaffolds would still provide sufficient mechanical support for tissue growth.

2.2 Materials and Methods

2.2.1 Hydrogel Preparation

The printing ink was prepared by dissolving 2% sodium alginate (Spectrum Chemical Mfg. Corp. Gardena, CA) into deionized (DI) water. A magnetic stir plate was used to mix the solution at room temperature until it became homogenous. The solution was then stored at 4°C in a refrigerator for at least 24 hours. The 2% calcium chloride ($CaCl_2$) crosslinker was prepared by dissolving 2g of $CaCl_2$ dihydrate powder (Fisher Scientific, Fairlawn, NJ) to 100mL of DI water and mixing it with the magnetic stir plate.

2.2.2 Modular 3D Printer

A custom modular 3D printer was designed and built for 3D printing, crosslinking, and directional freezing (See Figure 2.2). Each of the three processes took place on a separate module that could be rearranged to change the order of fabrication. For example, the crosslinking module could be switched with the directional freezing module so that directional freezing occurred first, or vice versa. As stated earlier, the first goal of this study was to investigate whether crosslinking should occur before or after directional freezing. The second goal was to investigate the influence of both rapid and slow cooling rates on the shape and size of the directional pores. To investigate these variables, the alginate strands were prepared using four possible treatments. The first option was crosslinking then rapid freezing at 0.5 degrees/second (CL-FR Rapid). The second option was crosslinking then slow freezing at 0.02 degrees/second (CL-FR Slow). The third option was rapid freezing at 0.5 degrees/second then crosslinking (FR-CL Rapid), and the fourth option was slow freezing at 0.02 degrees/second then crosslinking (FR-CL Slow). In addition, control strands were fabricated by printing and then crosslinking directly after, with no use of directional freezing.

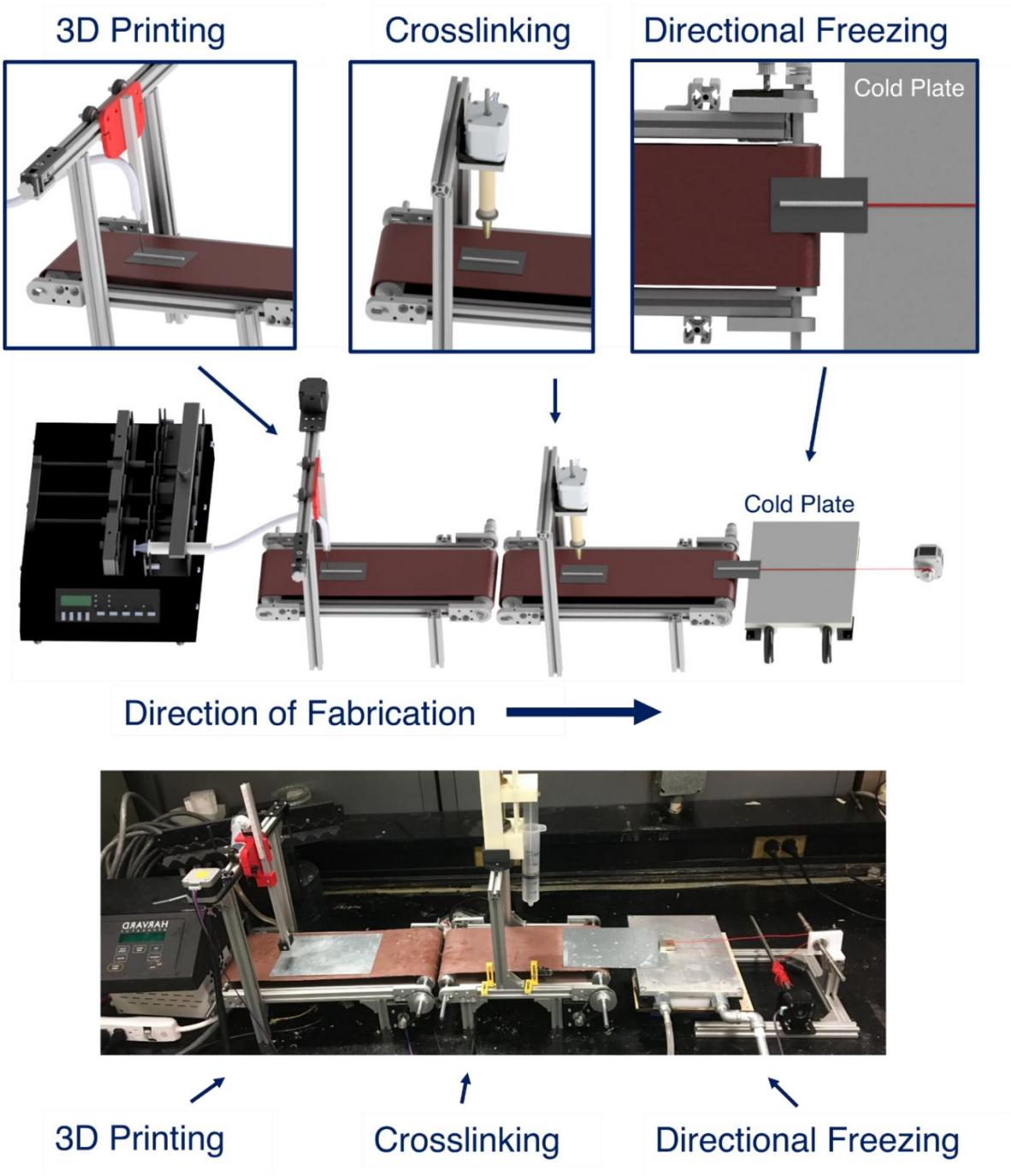

Figure 2.2 The modular 3D Printer, including the 3D printing, Crosslinking, and Directional Freezing modules. The Crosslinking and Directional Freezing modules can be switched depending on the desired order of fabrication.

2.2.3 3D Printing Module

The 3D printing module consisted of syringe pump extruder printing onto a conveyor belt. The syringe pump extruder with a 60cc syringe, and extrusion was powered by a Harvard PHD 2000 Syringe Pump (Hollington, MA, US). 2% sodium alginate at room temperature was pushed from the syringe through a plastic tube and down through a 12-gauge metal nozzle (2.16mm diameter). The nozzle moved back and forth on a belt along the y-axis, and deposited sodium alginate onto a print plate on the conveyor belt, which moved along the x-axis. To simplify analysis of factors affecting pore creation, single strands of sodium alginate were printed. The strands were 150 mm long and 2.5mm wide and printed at a speed of 15mm/second. When printing finished, the conveyor belt carried the print plate along the x-axis and onto the next module.

2.2.4 Crosslinking Module

For sodium alginate to achieve the required mechanical characteristics for tissue engineering, it must be ionically crosslinked by a crosslinker such as $CaCl_2$ after printing. The crosslinking module consisted of a conveyor belt moving along the x-axis and a stationary sprayer above the belt. The sprayer consisted of a custom syringe pump extruder attached to an atomizer, which sprayed a heavy mist of $CaCl_2$ droplets. As the print plate traveled down the conveyor belt, it stopped under the sprayer, and the printed object was sprayed thoroughly with 2% $Cacl_2$. The print plate remained stationary for ten minutes as crosslinking occurred, and then the conveyor belt pulled the print plate towards the next module.

2.2.5 Directional Freezing Module

During the directional freezing process, the print plate was pulled at a fixed rate across a room temperature plate to a cold plate. This resulted in ice crystal growth along the x-axis, from the cold plate towards the room temperature plate. The print plate was attached to a string that was wound around a pulley and driven by a stepper motor (See Figure 2.2). The cold plate was a CP3001 Wieland Microcool liquid-cooled cold plate, and either liquid nitrogen or ethylene glycol was circulated through the plate as the cooling fluid (Decatur, Al, US). For the rapid freezing process, liquid nitrogen was circulated through the cold plate with the surface of the plate reaching temperatures of -196°C. For the slow freezing process, a 45% ethylene glycol and water solution was circulated through the plate by a Neslab RTE-140 Cooling Bath, and six CP68475H-2 Peltier elements were placed on top of the cooling plate, with a resulting surface temperature of -40°C (Thermo Scientific, Waltham, MA, US, CUI Devices, Lake Oswego, OR USA) The temperature of the print plate in proximity to the alginate strands was measured throughout the freezing process with a K type thermocouple. The resulting cooling rate of the alginate strands for the rapid freezing process was approximately 0.5 degrees/second and the cooling rate for the slow freezing process was approximately 0.02 degrees/second. After completion of both the crosslinking and freezing processes, the resulting alginate strands were cut into uniform pieces for imaging and testing.

2.2.6 Surface Characterization

Due to the transparency of the alginate strands, it was possible to view the pores under a Nikon Eclipse TE300 inverted microscope (Nikon, Tokyo, Japan). The samples were untreated before being viewed in the inverted microscope and ImageJ was used to calculate the true size of the pores (NIH, US). SEM imaging was done using a Hitachi TM-4000 Scanning Electron Microscope (Hitachi, Tokyo, Japan). The samples were fixed in 2% glutaraldehyde with a 0.1M Sodium cacodylate buffer (pH 7.2). After ethanol dehydration they were dried in a Tousimis AutoSamdri 815 critical point dryer for an hour (Rockville, MD, US).

2.2.7 Tensile Testing

Uniaxial tensile testing was conducted at room temperature using an Instron® 5940 tensile testing machine (Instron, Norwood, MA, US). To enhance gripping during the test, the ends of the alginate strands were glued between squares of sandpaper. The hydration of the strands was maintained by storing them in a $CaCl_2$ bath up until testing. As testing temperature and testing speed affect the measured tensile properties of polymers, all samples were tested at the same temperature and testing speed. Testing was performed at a speed of 15mm per minute, and tensile tests were conducted with ten different samples for each treatment, including a control group. The ultimate tensile strength (MPa) was defined as the peak stress on the stress-strain graph.

2.2.8 Texture Profile Analysis

A Texture Profile Analysis is a type of compression test developed by the food industry to evaluate the textural properties of food. During a Texture Profile Analysis, a probe descends at a set rate through a sample and then retracts. We evaluated the firmness and work to shear of the alginate strands using a TA-XTPlus texture analyzer (Texture Technology Corp., Scarsdale, New York, US) with a TA-47 Lexan blade and a 1kg load cell. The strands were oriented perpendicular to the TA-47 blade on a Lexan base. The blade descended through the strands at 1mm/s until it touched the base, reached a threshold force, and retracted to finish the test. Tests were performed at room temperature and the samples were submerged in a $CaCl_2$ bath until testing to maintain hydration. Seven strands were tested for each treatment and each strand was tested in three different places. Firmness (N), which is also referred to as hardness or deformation force in the literature, corresponded to the maximum force noted in the force/time graph. The work required to shear the sample (N*m) corresponded to the area under the curve.

2.2.9 Statistical Analysis

Comparison between means was made using a Student's T-test with a significance level set at $p < 0.05$. Data points more than two standard deviations from the mean were removed.

2.3 Results and Discussion

2.3.1 Surface Characterization

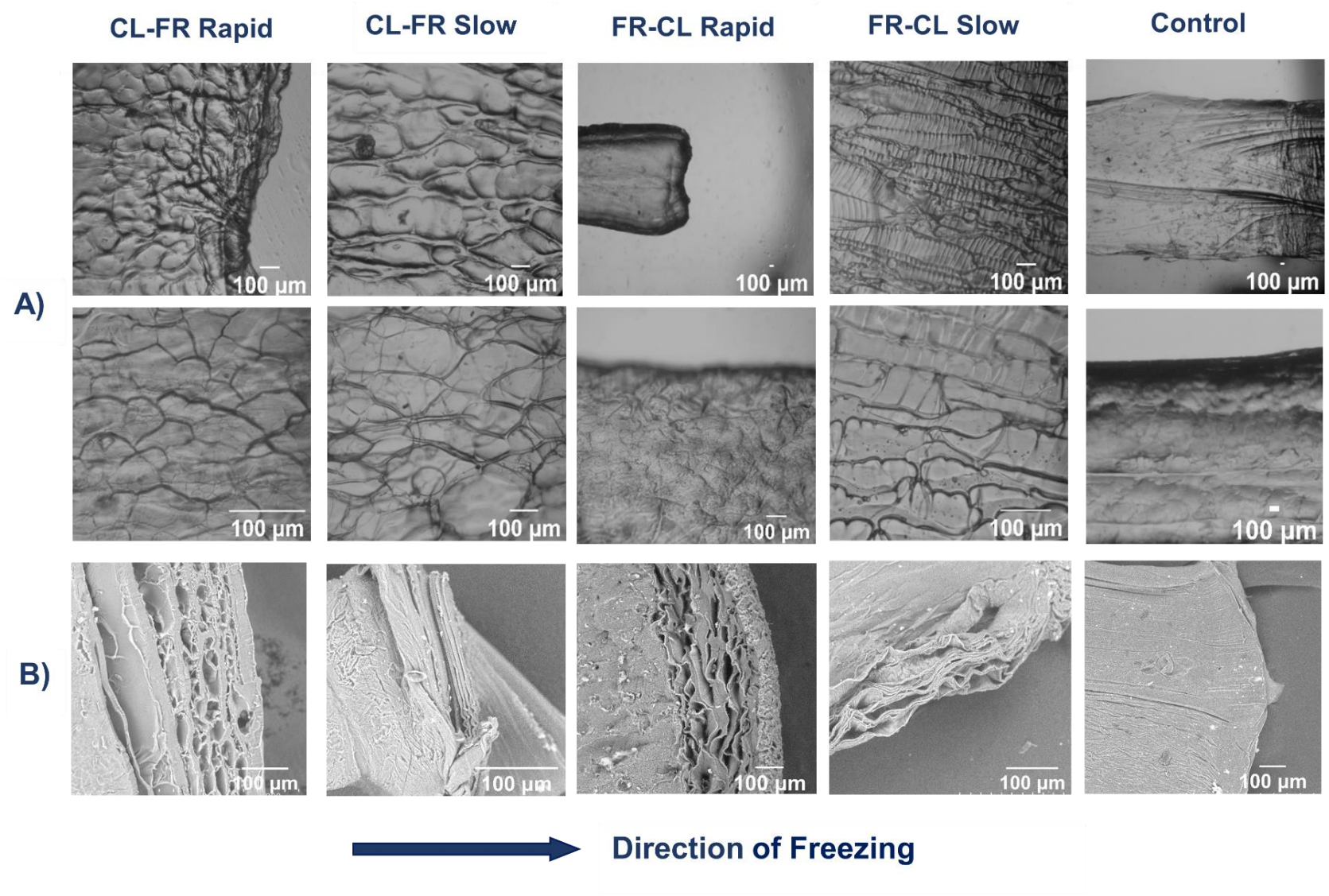
CL-FR Rapid
CL-FR Slow
FR-CL Rapid
FR-CL Slow
Control
A)
B)
100 µm
Direction of Freezing

Figure 2.3 A) Inverted microscope images of the alginate strands taken from a top view. B) SEM images of cross-sections of the alginate strands.

Directional pores were visible in the CL-FR Rapid, CL-FR Slow, and FR-CL Slow strands, with pores in the CL-FR Rapid and CL-FR Slow strands showing high interconnectivity. Pores in the FR-CL Rapid strands were not visible under the inverted microscope, but SEM images of cross-sections revealed that pores existed. It is possible that freezing process altered the surface of the FR-CL strand, making it opaque and preventing the pores from being visible under the inverted microscope. As expected, no pores were visible in the control strands.

The visible pores created by directional freezing ranged from a 5 μm diameter in the CL-FR Rapid strands to 40 μm diameter in the CL-FR Slow pores. This difference in size between the pores in the slow cooled and rapid cooled strands is consistent with theory and results from the literature. High freezing temperatures and a long time for crystallization produce large ice crystals, while low freezing temperatures and a quick time for crystallization produces smaller, finer crystals [54, 64]. Malecki et al., and Nishihara et al., used directional freezing in gels and found that larger pores were produced by a low cooling temperature and low cooling rate [51,56]. The observed pores were on the proper scale for cell growth [65]. According to tissue regeneration studies, 5 μm is an optimal pore size for neovascularization 5-15 μm is optimal for fibroblast ingrowth, 20-125 μm is optimal for adult skin, 100-350μm is optimal for bone regeneration, and 40-100 μm is optimal for osteoid ingrowth [66]. Thus, by controlling the cooling rate, different size pores can be created for different types of cell growth. Larger pores could likely be created by further slowly the cooling rate, and macropores can be created using the 3D printing process.

An interesting phenomenon observed here was the difference in ice crystal pattern between the CL-FR and the FR-CL strands. The CL-FR strands displayed highly interconnected pores, while in contrast, the FR-CL slow strands displayed dendritic pores with long columnar primary dendrites and evenly spaced secondary dendrites. Faster cooling rates are expected to produce smooth primary dendrite arms that are spaced quite close together and have relatively little secondary dendrite growth, while slow cooling rates are expected to produce primary dendrite arms that are farther apart and have more secondary dendrite growth [67]. Interestingly, this effect is seen in the FR-CL slow pores but not in the CL-FR slow pores. Ultimately, the highly interconnected pores viewed in the CL-FR strands are preferable for cell growth over the more parallel, spaced-out pores viewed in the FR-CL slow strands.

2.3.2 Tensile Testing

If 3D printed scaffolds for tissue engineering do not have enough mechanical strength to maintain their shape during cell proliferation, the emerging tissue will be deformed [68]. Porosity and pore size greatly affect the mechanical properties of porous hydrogels, so it is critical to evaluate if these hydrogels have sufficient mechanical strength [68]. Here, we used uniaxial tensile testing to compare control strands with strands that have undergone various types of directional freezing.

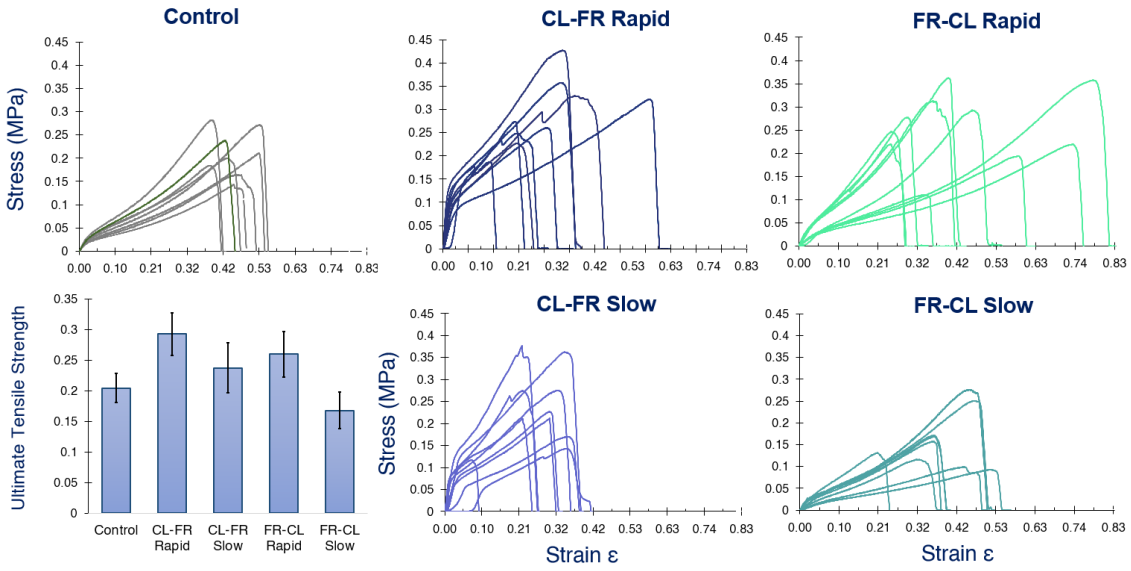

Figure 2.4 A) Stress-Strain curves for Control strands, CL-FR Rapid, FR-CL Rapid, CL-FR Slow, and FR-CL Slow treatments. Tensile testing was conducted on ten samples for each treatment. B) Average ultimate tensile strengths of all treatments. Treatments in group a) are statistically significant difference from the Control strands while treatments labeled in group b) are statistically significant difference. Error bars represent +/- one standard deviation from the mean.

Treatment	Tensile Strength (MPa)
Control	0.204 ± 0.047
CL-FR Rapid	0.292 ± 0.069
CL-FR Slow	0.237 ± 0.082
FR-CL Rapid	0.260 ± 0.074
FR-CL Slow	0.168 ± 0.059

Table 2.1 Mean and standard deviations from tensile testing

As reported in Table 1., all strands had an ultimate tensile strength above 0.16 MPa, and the ultimate tensile strength of the CL-FR Rapid, CL-FR Slow, and FR-CL Rapid strands was higher than the control strands (See Figure 2.4). A student's T-test found that the increase in tensile strength between the CL-FR Rapid and the control strands was statistically significant, but the

other treatments were not significantly different from the control strands. Thus, we can conclude that the use of directional freezing will not decrease the tensile strength of a sodium alginate scaffold as to prevent it from being usable in the body. In fact, some directional freezing treatments can marginally increase the tensile strength of a sample. It is possible that the increase in strength in the CL-FR Rapid strands is due to the directionality of the pores. Liu et al found that directionally freeze-thawed GO-PVA hydrogels had a higher tensile strength than freeze-thawed GO-PVA hydrogels and theorized that the increase in strength was due to the organized network of hydrogel created by directional freezing [69]. The range of tensile strengths measured here is also consistent with the tensile strength of 2% sodium alginate that is reported in the literature, although different testing speeds were used. Fu et al tested six grades and ten batches of 2% sodium alginate and found ultimate tensile strengths between 0.123 MPa and 0.679 MPa [70].

It is important to note that the tensile strength of 2% sodium alginate strands is significantly less than the tensile strength of normal human skin, which has an ultimate tensile strength of 7.7 MPa [68]. There are various ways of modifying sodium alginate to achieve tensile strengths that are closer to human tissue. For example, the addition of materials such as graphene oxide or poly (lactic- co-glycolic acid) PLGA can increase the mechanical strength of alginate scaffolds [71,59]. Submerging samples in a bath of crosslinker for an extended time period, such as for two weeks, can also improve mechanical strength [72]. While the alginate strands prepared here have a tensile strength that is significantly lower than human skin, ultimately the tissue-engineered scaffold is not intended to act as a permanent replacement for native tissue. Rather, it is needed to withstand temporary expansive and contractive forces in a wound or during cell growth [68].

2.3.3 Texture Profile Analysis

A Texture Profile Analysis was used to evaluate the extent to which directional freezing treatments altered the mechanical properties of the sodium alginate strands. Previously, Hurler et al., proposed the use of Texture Profile Analysis as a fast and reproducible method of characterizing hydrogels and determining their potential for wound therapy [73]. A sample's firmness and work to shear represent its resistance to deformation in the body [73]

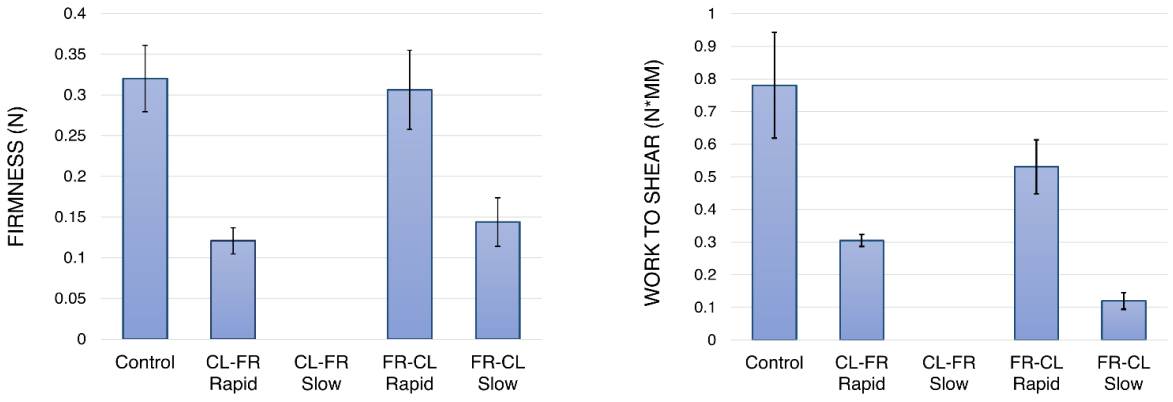

Figure 2.5. Bar Graphs for Firmness and Work to Shear. Error bars represent +/- one standard deviation from the mean.

Treatment	Firmness (N)	Work to Shear Sample (N*m)
Control	0.320 ± 0.082	0.780 ± 0.323
CL-FR Rapid	0.121 ± 0.033	0.305 ± 0.037
CL-FR Slow	NA	NA
FR-CL Rapid	0.272 ± 0.056	0.531 ± 0.165
FR-CL Slow	0.144 ± 0.059	0.120 ± 0.051

Table 2.2 Means and standard deviations for Firmness and Work to Shear

Unlike the tensile strength of the samples, which increased with the addition of a directional freezing process, directional freezing decreased the firmness of alginate strands. This is not unexpected, as increases in the porosity of hydrogels typically decreases the hydrogel's mechanical strength [74, 63]

The CL-FR Slow strands had such a loss in firmness that they could not be tested with the TA-XTPlus texture analyzer. Thus, while CL-FR Slow displayed large and highly interconnected pores, the loss in mechanical strength may prevent this treatment from producing useful tissue-engineered scaffolds. The firmness and work to shear of CL-FR Rapid and FR-CL Slow were significantly lower than the control strands, however, there was not a statistically significant difference between the FR-CL Rapid strands and the control strands. Likely, the loss of firmness in the slow-frozen strands is due to the larger pores that were created through the slow freezing process. If so, this suggests that the FR-CL strands have a lower porosity than the CL-FR strands, which is suggested as well by the tensile data and the microscope images. As with the tensile data, there is a statistically significant difference between the CL-FR and FR-CL treatments, which suggests that these two methods create different pore patterns.

2.4 Conclusion

In this study, we used a novel modular 3D printer to print, crosslink, and directionally freeze hydrogel strands for tissue engineering. By separating these processes onto three modules, we created a manufacturing system where the order of fabrication can be altered, and each process could take place using unique parameters. This modular technology not only aids fundamental studies but may also be valuable for the large-scale continuous manufacturing of biomaterials. The use of directional freezing coupled with 3D bioprinting created directional pores with diameters from 5 μm to 40 μm. Our first goal was to investigate how crosslinking before or after directional freezing impacted the creation of pores. Hydrogel strands that were crosslinked before undergoing directional freezing showed pore patterns with greater interconnectivity, while strands that were crosslinked after directional freezing displayed spaced out pores with less interconnectivity. Our second goal was to investigate the influence of both rapid and slow cooling rates on the size of the pores. As expected based on previous results, faster cooling rates resulted in smaller pores on the scale of 5 μm, and slower cooling rates resulted in larger pores on the scale of 40 μm. Thus, by altering parameters such as crosslinking and cooling rate, it is possible to control the pattern and size of the micropores. Our third goal was to evaluate the mechanical properties of the directionally frozen scaffolds and determine if they would still provide sufficient support for tissue growth. The directionally frozen strands had similar tensile strengths to the control strands and values reported in the literature. The strands which were crosslinked and then rapidly frozen had a higher tensile strength than the control strands, possibly due to the directional pores. The results from the texture profile analysis found that directionally freezing the scaffolds decreased their firmness and work to shear. In the case of strands that were crosslinked and slowly frozen, the loss in firmness and work to shear was significant, likely due to the large size of the pores. Further work with the modular 3D printer should evaluate scaffolds printed with cell-laden bioinks. Due to the modular nature of the printer, it will be possible to assess cell viability during each stage of the manufacturing process and to then tune parameters at each stage to avoid cell death. Additionally, to simplify analysis of the effects of various parameters on pore creation, only single strands of sodium alginate were 3D printed in this study. However, in future research the abilities of 3D printing can be further utilized to create customized pore morphologies, complex shapes, and multi-material structures [9]. In combination with directional freezing, 3D printing can thus be used to create complicated structures with both a macrostructure and a microstructure.

Chapter 3

3. Freezing-Modulated-Crosslinking

3.1 Introduction

3D cryoprinting is a promising method of printing objects out of soft bioinks and creating highly porous scaffolds for tissue engineering. However, crosslinking the frozen objects before they thaw and collapse remains a challenge. Here we investigate a process which we name “freezing-modulated-crosslinking” for crosslinking frozen objects produced by 3D cryoprinting. During freezing-modulated-crosslinking, frozen objects are thawed in a crosslinker bath at a controlled melting rate, so that crosslinking occurs layer by layer and the object can maintain its printed shape. First, we examine the process with a mathematical model to determine the important thermal parameters. Second, we validate our results experimentally by printing a variety of multi-layer alginate objects. By systematically examining this crosslinking approach, we expand the options for 3D cryoprinting. 3D cryoprinted alginate scaffolds can be seeded with cells for use in 3D cell culture or for tissue regeneration.

The low viscosity of alginate bioinks makes it easy to extrude through a small nozzle, however, in order for alginate objects to maintain their structure, they must almost always be crosslinked during or after printing. "Crosslinking" refers to the process of forming chemical bonds between polymer chains, making them more rigid. Alginate can be ionically crosslinked, chemically crosslinked, or enzymatically crosslinked among other methods [61]. The timing and rate of crosslinking is a significant challenge for printing alginate bioinks, because if crosslinking occurs before printing, the alginate will be too viscous to extrude through the nozzle, and if crosslinking occurs too long after deposition on the print plate the printed structure will collapse.

While 3D cryoprinting can be used to build rigid structures out of soft biomaterials, the challenge then becomes transforming these frozen, rigid objects into thawed scaffolds for use in tissue engineering. Many common crosslinking approaches used for 3D bioprinting cannot be used as the object is in a frozen state. Previously, photocrosslinking and internal gelation have been used to crosslink objects fabricated with 3D cryoprinting [46, 47, 74]. A drawback of internal crosslinking is that the bioink is only fluid enough to be extruded through the nozzle on the order of minutes before it becomes too viscous to be used. Additionally, reliance on photocrosslinking drastically reduces the number of bioinks that can be 3D cryoprinted as many materials are not

photo-crosslinkable. Options for crosslinking 3D cryoprinted objects remain limited, and innovation in this aspect could advance the field.

In Chapter 2, we studied the mechanical properties of single-layer cryoprinted alginate in two configurations, a) freezing followed by crosslinking during thawing and b) crosslinking followed by freezing. The mechanical analysis of the products found that the former method yields a material with higher firmness and greater work to shear [75]. This chapter investigates a method of crosslinking objects fabricated by 3D cryoprinting, which we name "freezing-modulated-crosslinking." This method involves the following steps (See Figure 3.6). First, during 3D cryoprinting, a low-viscosity alginate bioink is extruded through the nozzle and freezes as it is deposited on the print plate. After printing is complete, the frozen object can be stored in a freezer for short-term or long-term use. Then, when the scaffold is ready to be used, freezing-modulated-crosslinking is used to thaw the frozen object at a controlled rate inside a bath of crosslinker such that it maintains its initial shape. Finally, the scaffold can be used for tissue-engineering applications. For the purpose of this study, freezing-modulated-crosslinking will be investigated as a method of crosslinking frozen, a-cellular scaffolds. For this application, cells can be seeded into the scaffolds after fabrication is complete, similarly to the work of Dar et al. [76]. The challenge is to control the thawing rate of the frozen object, so that the rigidity provided by freezing is replaced by cross linking as the Ca+ ions diffuse into the thawed region. This technique is somewhat reminiscent of freeze substitution. Crosslinking alginate structures in a bath of $CaCl_2$ is a common crosslinking technique used in 3D bioprinting. However, to the best of our knowledge, this is the first time that temperature control of the $CaCl_2$ bath has been used to crosslink layer-by-layer in order to maintain the structure of a soft printed object. In addition, this is the first time the parameters of freezing-modulated-crosslinking have been investigated in order to optimize the structure of the printed object.

This paper has two parts, a mathematical analysis and an experimental validation. In the first part, a dimensionless analysis is used to determine what and how the thermal parameters control the process of freezing-modulated-crosslinking. Our mathematical analysis finds that two temperature parameters can be used to control the process: the surface temperature of the melting object and the initial temperature of the frozen sample. In the second part, we qualitatively examine the effect of these parameters by printing various shapes out of 2% sodium alginate and crosslinking them in a $CaCl_2$ bath with freezing-modulated-crosslinking. To further characterize freezing-modulated-crosslinking, we also examine the impact of $CaCl_2$ concentration. The results demonstrate the feasibility of this technique and qualitatively confirms the predictions of the mathematical model. The development of freezing-modulated-crosslinking expands the type of biomaterials that can be used for 3D cryoprinting and the type of structures that can be printed out of soft bioinks.

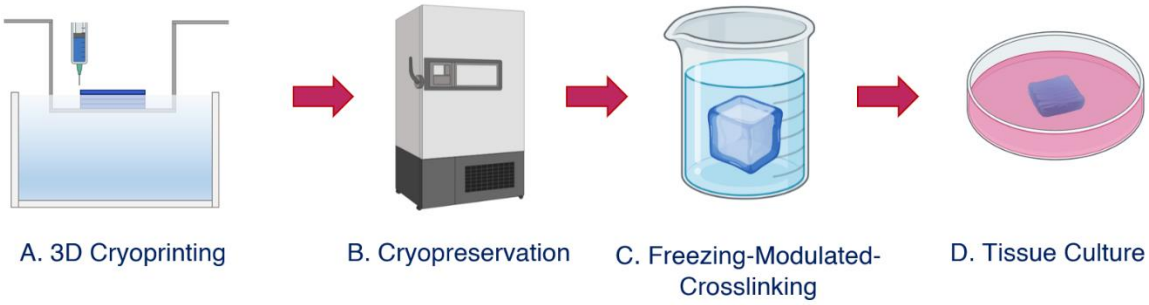

Figure 3.1 A) 3D Cryoprinting B) The scaffold is kept frozen for either short-term or long-term preservation. C) The object is crosslinked using freezing-modulated-crosslinking. D) The object is ready for tissue culture.

3.2 Freezing-Modulated-Crosslinking

Crosslinking sodium alginate with $CaCl_2$ is simple and cost-effective method of increasing the mechanical strength of alginate bioinks [77]. When alginate is in the presence of $CaCl_2$, the Ca^+ ions bind to the guluronate blocks of the alginate chains, and form junctions between guluronate blocks on adjacent alginate chains [78]. The junctions between the alginate chains create a three-dimensional network, increasing the rigidity of the polymer (See Figure 3.7A). During freezing-modulated-crosslinking, the frozen alginate object is immersed in a chilled bath of $CaCl_2$ at a temperature slightly above the melting temperature of alginate. The printed object melts layer by layer, allowing the Ca^+ ions to diffuse into the melted region and crosslink the alginate (See Figure 3.7B-C). Thus, by controlling the speed of the melting interface on the object it is possible to control the crosslinking interface as well. By melting only a thin layer at a time while the rest of the object remains frozen, the printed object is able to maintain its original shape and prevent collapse. Control of the melting rate is critical to this approach and will be discussed in detail in the mathematical analysis and in the results section.

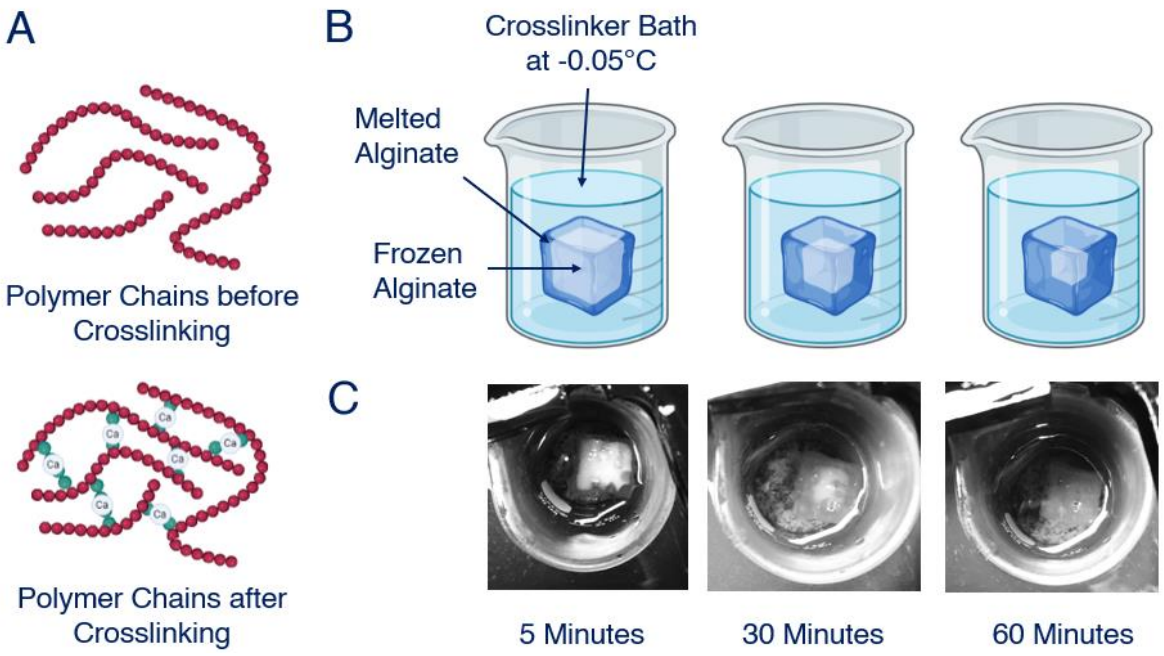

Figure 3.2 Freezing-Modulated-Crosslinking. A) During crosslinking, Ca^{+} ions link alginate chains, creating a 3D network and increasing the rigidity of the polymer. B) Freezing-modulated-crosslinking

3.3 Mathematical Model

During freezing-modulated-crosslinking, the crosslinker solution melts the frozen object and the Ca^{+} ions diffuse into the melted region to crosslink the alginate and provide mechanical integrity. The process is illustrated in Figure 3.8 which shows the melting interface propagating into the frozen object, followed by the crosslinking interface. Thermal diffusivity is significantly larger than mass diffusivity. Ideally, the melting interface will precede slightly the crosslinking reaction interface, in such a way that the structural rigidity provided by the ice will be replaced by the crosslinking structural rigidity. The goal of this dimensionless mathematical analysis is to generate a qualitative understanding about how the different process parameters can be controlled to obtain the design goal.

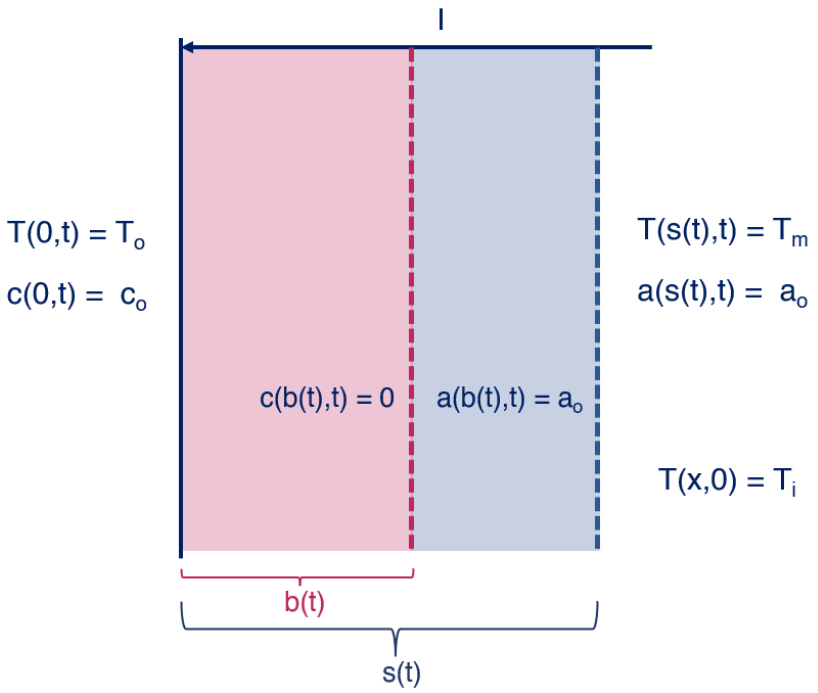

Figure 3.3 Movement of the melting interface, s(t), and the crosslinking interface, b(t).

In this model, we assume that we analyze the crosslinking of a semi-infinite domain, initially at a temperature T_o, while immersed in a solution of $CaCl_2$ with a calcium concentration of c_o and a temperature of T_o. We also assume good mixing in the solution that surrounds the frozen surface. A similar analysis could be performed with heat and mass transfer convection boundary condition.

Additionally, it is assumed that complete crosslinking occurs at the interface b(t) and that the calcium is completed depleted during crosslinking. The concentration of alginate in the thawed region is assumed to be constant and there is no diffusion of alginate in the crosslinked volume. This assumption is based on reports from experimental studies which state that: "it is evident that the diffusion of free alginate molecules in the gel phase is severely restricted" [79]. It is further assumed that complete melting occurs at the melting interface s(t), which is at the phase transition temperature, T_m. The system is at an initial temperature, $T_i(x, 0)$, which is also the temperature far away from the melting interface. The outer surface temperature is, $T_o(0, t)$ and the outer surface concentration of Ca ions is $c_0(0, t)$

The governing equations are the heat and mass transfer equations, and the moving boundaries are defined by conservation of mass at the crosslinking reaction boundary and conservation of energy at the melting boundary.

We dimensionalized the energy equations in the liquid (l) and frozen domains (f) and the mass transfer equation using the following dimensionless variables:

[1]

$$\theta = \frac{T_0 - T}{T_0 - T_m}\ ;\ \zeta = \frac{x}{l}\ ;\ \tau = \frac{\alpha_l t}{l^2}\ ;$$
$$C = \frac{c_0 - c}{c_0}\ ;\ A = \frac{a_0 - a}{a_0}\ ,$$
$$S = \frac{s(t)}{l};\ B = \frac{b(t)}{l}$$

Where, l, is an arbitrary dimension which could be the desired depth of cross linking or a dimension unit.

The energy equation in the molten region is given by:

$$\frac{\partial \theta_l}{\partial \tau} = \frac{\partial^2 \theta_l}{\partial \zeta^2}\ 0 < \zeta < \frac{s(t)}{l} \quad [2]$$

The energy equation in the frozen region is given by:

$$\frac{\partial \theta_f}{\partial \tau} = \frac{\alpha_f}{\alpha_l}\frac{\partial^2 \theta_f}{\partial \zeta^2}\ \zeta > \frac{s(t)}{l} \quad [3]$$

The dimensionless energy equation on the melting interface is given by:

$$-\frac{\partial \theta_l}{\partial \zeta} + \frac{k_f}{k_l}\frac{\partial \theta_f}{\partial \zeta} = \frac{1}{Ste}\frac{dS(\tau)}{d\tau}\ on\ S\ =\ \frac{s(t)}{l} \qquad [4]$$

Where, $\alpha_f,\ k_f,\ c_f$ are the thermal diffusivity, thermal conductivity, and heat capacity in the frozen region respectively and $\alpha_l,\ k_l,\ c_l$ are the thermal diffusivity, thermal conductivity and heat capacity in the melted (liquid) region respectively.

The dimensionless initial and boundary conditions are:

[5]

$$\theta_f(\zeta, 0) = \frac{T_i - T_o}{T_m - T_o} = V = \theta_f(\infty, t);\ S(0) = 0$$

$$\theta_l(0, t) = 0 : \theta_l\ (s(t), t) = \theta_f\ (s(t), t) = \frac{T_m - T_o}{T_m - T_o} = \theta_m = 1 : \theta_f(\infty, t) = V$$

Equation [4] shows the emergence of a dimensionless number known as the Stefan number (Ste) which actually governs the behavior of the solution.

$$Ste = \frac{c_l\ (T_0 - T_m)}{L}$$

[6]

Typically, the Stefan number for problems of phase transformation with water, is smaller than 1, which leads to the so-called steady state approximation which will be discussed later.

The dimensionless mass equation for the Ca diffusion problem is:

$$\frac{\partial C}{\partial \tau} = \frac{1}{Le_c}\frac{\partial^2 C}{\partial \zeta^2} \; 0 < \zeta < \frac{b(t)}{l} \qquad [7]$$

Where the Lewis number is given by:

$$Le_c = \frac{\alpha_l}{D_c} \qquad [8]$$

The location of the crosslinking interface is found by equating the flux of calcium ions across the crosslinking interface and the kinetics of cross linking, Ψ. The reaction kinetics terms were discussed in many publications, e.g. [80], [81], [82], and [83]. According to Kim et al., and Mikkelsen et al., $\Psi = \Psi(\kappa, p, q)$, where κ, is a measure of the reaction kinetics rate, p, is the concentration of the sodium alginate solution and q, is the number of moles of calcium binding per gram of alginate [80, 81]. There are several other ways to define Ψ as in Mikkelsen et al., and Braschler et al [81, 84]. In this study we will assume that Ψ is dependent on the parameters defined by Kim et al., and Mikkelsen et al, which means that it has units of concentration of alginate.

The dimensionless equation on the crosslinking boundary is:

$$-\frac{\partial C}{\partial \zeta} = Le_c \frac{\Psi}{c_0}\frac{dB}{d\tau} \qquad [9]$$

The boundary and initial conditions become:

$$C(0,\tau) = 0 \; C(B,\tau) = 1, \; B(0) = 0 \quad [10]$$

The problems to be solved are the energy equations [2], [3], [4] with boundary and initial conditions [5] and the mass transfer equations [7], [9] [15]. These problems are mathematically known as Stefan like problems and examination of the equations and conditions above, leads to the realization that these problems are of the Newman type, which are the only phase transition, chemical reactions problems with a moving interface that have an exact solution. The exact solution and its derivation can be found in Carslaw et al; Ch 11 [85]. Since we are interested

primarily in the propagation of the mass transfer boundary relative to the heat transfer boundary, we will list here only the solution for the motion of these interfaces.

The propagation of the melting interface is given by Carslaw et al.

$$S(\tau) = 2\lambda(\tau)^{\frac{1}{2}} \quad \text{or in dimensional form, } s(t) = 2\lambda(\alpha_l t)^{\frac{1}{2}} \quad [11]$$

The value of λ for water and ice was calculated and tabulated [85]. For the dimensionless analysis here, the tabulated data becomes:

V-1 =	0	1	2	3	4	5
$\theta_m = 1$	0.056	0.054	0.053	0.051	0.050	0.049

Where $$V - 1 = \frac{T_m - T_1}{T_0 - T_m} \quad [12]$$

V-1 is the ratio between the difference of the initial and the melting temperature and the outer surface temperature and the melting temperature. Obviously the larger the difference the slower is the propagation of the melting interface. This is a design consideration in our technique; to slow down the propagation of the melting interface the larger must be the ratio in equation [12], Note that the case V-1 = 0 is when the initial temperature is the phase transition temperature. This particular case, in which the initial temperature is the melting temperature, and in which the Ste is small, lends itself also to an approximate solution, known as the quasi-steady solution [86].

In this case, the energy equation reduces to

$$0 = \frac{\partial^2 \theta_l}{\partial \zeta^2} \; 0 < \zeta < \frac{s(t)}{l} \quad [13]$$

The temperature in the liquid region becomes:

$$\theta_l = (1 - \frac{\zeta}{S}) \; for \; 0 < \zeta < S \quad [14]$$

And the solution of the energy equation at the melting interface yields,

$$S = \sqrt{2 \; Ste \; \tau} \quad [15]$$

The thermal diffusivity of water at room temperature of $1.4 \times 10^{-7}\, m^2/s$ and a mass diffusivity of calcium estimate of $1.2 \times 10^{-9}\, m^2/s$ suggests that the Lewis number for this problem is $Le(O) = 100$. At the time scale when the temperature distribution in the liquid phase is assumed quasi steady, the calcium concentration distribution concentration profile identified by a Lewis number on the order of 100, can be also assumed quasi-steady. It should be emphasized that this assumption was also done by others, e.g. Kim et al [80].

In the quasi-steady case, the mass transfer equation becomes.

$$\frac{\partial^2 C}{\partial \zeta^2} = 0 \; 0 < \zeta < \frac{b(t)}{l} \quad [16]$$

And the solution gives the concentration of calcium ions profile

$$C = (1 - \frac{\zeta}{B})\, for\; 0 < \zeta < B \quad [17]$$

The conservation of mass equation on the crosslinking interface becomes

$$\frac{1}{B} = \Gamma \frac{dB}{d\tau} \quad [18]$$

Where:

$$\Gamma = Le_c \frac{\Psi}{c_0} \quad [19]$$

The solution for the propagation of the dimensionless cross linking interface B becomes very similar in form to the equation for the propagation of the melting interface, with the new dimensionless number Γ, replacing the Stefan number (Ste)

$$\mathrm{B} = \sqrt{2\Gamma\tau} \quad [20]$$

It should be emphasized that this solution for B is independent on the propagation of melting interface, S.

The goal of this study is to find ways to control the relative distance between the crosslinking interface and the phase transition interface. We have found earlier that the propagation of the phase of change interface can be controlled through the ratio given in [12]. Now, equations [15] and [20] suggest the variable parameters that can be used to affect the distance between the crosslinking interface and the phase transition interface. Interesting the ratio between B and S gives a new dimensionless number that can be used for this purpose.

$$\frac{B}{S} = \sqrt{\frac{\Gamma}{Ste}} = W \quad [21]$$

This ratio in a dimensional form becomes:

$$\frac{b(t)}{s(t)} = \{\frac{\alpha_l \psi L}{D_c c_o [c_l (T_0 - T_m)]}\}^{1/2} \quad [22]$$

This equation suggests that decreasing $(T_0 - T_m)$, will increase b(t) relative to s(t)

This analysis suggests that it is possible to control the relative propagation of the crosslinking interface to the phase transition interface through control of two thermal terms; $(T_0 - T_m)$ and $\frac{T_m - T_1}{T_0 - T_m}$

Thus, the goal of the following experimental section is to demonstrate the feasibility of freezing-modulated-crosslinking as a technique and to evaluate how these two thermal terms will affect the outcome of the cryoprinting process.

3.4 Experimental Materials and Methods

3.4.1 The 3D bioprinter

An Ender-5 Plus extrusion-based printer was modified for 3D cryoprinting with the addition of a custom syringe extruder, print plate, and cooling bath (See Figure 3.9). The cooling bath contained a 45% ethylene-glycol and water solution that was continuously circulated by a Neslab RTE-140 Refrigerated Circulator (Thermo Scientific, Waltham, MA). The solution was circulated from the Neslab RTE-140 through tubes connecting to the cooling bath of the 3D printer, which could then achieve temperatures between -30°C and 23°C, although printing at -15°C yielded the best print results. During printing, biomaterial was extruded through a nozzle onto the print plate, which then descended downward by the height of the printed layer, such that the top layer remained a fixed distance from the cryogenic fluid (See Figure 3.9B). Thus, the material at the tip of the nozzle was extruded at an identical temperature for each layer. This is notable for two reasons. First, by printing each layer at the same temperature, the printed object is expected to have uniform properties. Second, for cell-laden bioinks, all cells should be kept at specific thermal conditions to maximize cell survival. Currently, the majority of 3D cryoprinters involve printing onto a cooled plate at a static temperature. A drawback to this approach is that the temperature of the printed material increases as the layers of the printed object grow higher. As a result, the bottom

layer of the object is printed under different thermal conditions than the highest layer. The 3D cryoprinter used in this study avoids this issue, as the print plate descends further into the cryogenic fluid after each layer, keeping the temperature at the nozzle fixed.

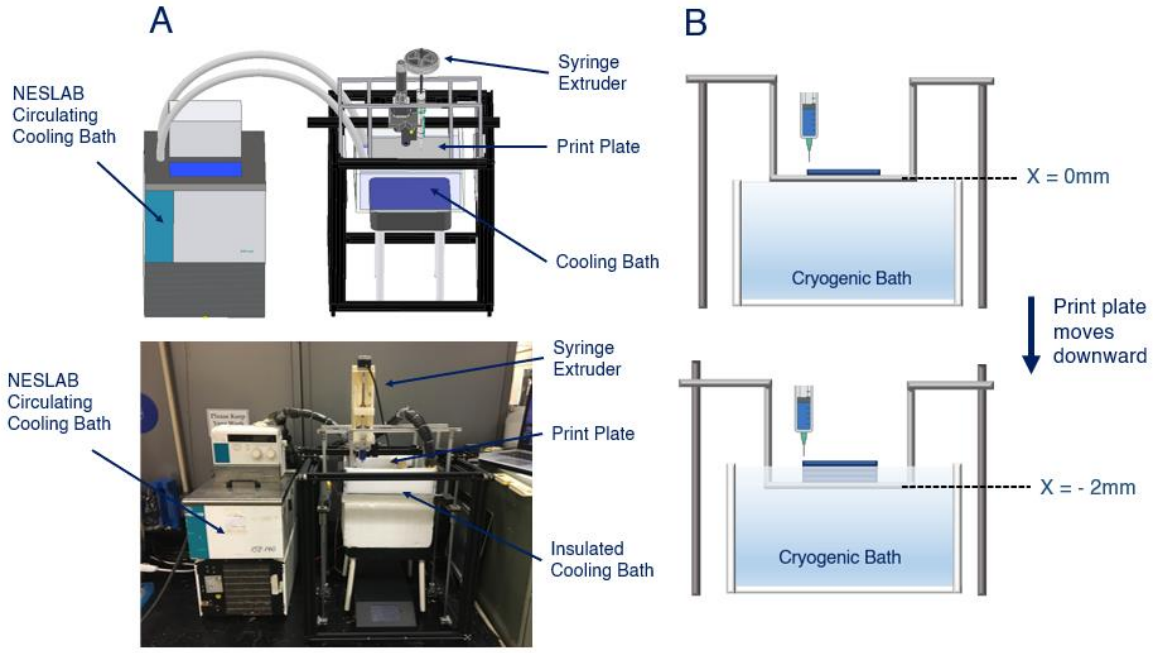

Figure 3.4 A. The 3D Cryoprinter. B. Printing the first layer of an object. After finishing the layer, the print plate descends further into the cooling bath such that the temperature at the layer being printed is constant.

3.4.2 Printing Parameters

2% sodium alginate was used as the printing ink. The ink was produced by dissolving 2% sodium alginate (Spectrum Chemical Mfg. Corp, Gardena, CA) into de-ionized water. The solution was mixed at room temperature with a magnetic stir plate until it became homogenous and was then stored in a 4C refrigerator for 24h. For photographing the printed objects, blue dye was added to the ink to create increased visual contrast (Watkins, Winona, MN). The abilities of the 3D cryoprinter and freezing-modulated-crosslinking method were demonstrated by 3D printing and crosslinking cubes, rings, and lattices. The bioink was extruded by a custom syringe extruder through an 18-gauge nozzle. The printing speed was 10mm/second, and the temperature of the newly printed layer was fixed at -15°C.

3.4.3 The Crosslinker Bath

Baths of 2%, 4%, or 6% $CaCl_2$ crosslinker were prepared by dissolving 2g, 4g, or 6g of $CaCl_2$ dihydrate powder (Fisher Scientific, Fairlawn, NJ) in 100mL of de-ionized water. A magnetic stir plate was used to mix the solution until it was homogenous. 5% concentration of Pluronic™ F-68 Non-ionic Surfactant was added to the solution to prevent surface forces from distorting the melting interface and thus changing the shape of the printed object (Thermo Scientific, Waltham, MA). The crosslinker solution was then poured into a glass beaker, which was suspended inside the internal cooling bath of the Neslab RTE-140 Refrigerated Circulator. The internal cooling bath of the Neslab RTE-140 circulated a 45% ethylene-glycol and water solution and could produce temperatures between -45°C and 30°C. The solution was then circulated through tubes that attached to the 3D printer's cooling bath. Based on insights from both the mathematical model and experimental results, the temperature of the crosslinking solution was kept at various temperatures between -4°C and 5°C. Before the frozen alginate object was dropped into the crosslinker, it was kept at either -20°C or -80°C. The optimal temperatures for both the frozen object and the crosslinker bath will be discussed in the results section.

3.4.4 SEM Images

SEM imaging was taken with a Hitachi TM-4000 Scanning Electron Microscope (Hitachi, Tokyo, Japan). The sodium alginate objects were fixed in 2% glutaraldehyde with a 0.1M Sodium cacodylate buffer (pH 7.2). After ethanol dehydration, the objects were dried using a Tousimis Auto-Samdri 815 critical point dryer for one hour (Rockville, MD).

3.4.5 Image Analysis and Statistical Analysis

Images of the 3D cryoprinted lattices were analyzed in ImageJ (NIH, US) to determine the size of the pores. The size of five pores in each of three lattices were analyzed for every set of temperature or concentration parameters. A Student's T-test was used to compare the means with a significance level set at $p < 0.05$. Data points more than two standard deviations from the mean were removed.

3.5 Results and Discussion

3.5.1 Optimizing Thermal Parameters

The mathematical model identified that it is possible to control the propagation of the crosslinking interface by controlling two terms, the initial temperature of the frozen object and the

temperature of the crosslinker bath. By varying these two terms, we examined their effect on the outcome of the printed objects undergoing freezing-modulated-crosslinking. The goal of this experiment was to maximize "object accuracy," aka how closely the crosslinked object resembles the intended object in size and shape. Thus, the optimal initial object temperature and crosslinker bath temperature were considered those that produced a crosslinked object which most closely resembled the intended object. 3D cryoprinted lattices were crosslinked under various thermal conditions by varying the object temperature and the temperature of the crosslinker bath (Figure 3.10.) Based on the Gcode used to print the lattices, the theoretical pore size of a 3D cryoprinted lattice was $1mm^2$. All lattices that underwent freezing-modulated-crosslinking displayed shrinkage. Up to 50% shrinkage is expected for alginate objects crosslinked with $CaCl_2$, [87, 88]. However, objects that were melted at faster rates displayed increased shrinkage when compared to those melted at slower rates. The difference in shrinkage between lattices crosslinked at room temperature aka 20°C (Groups A and B) and lattices crosslinked at -0.05°C (Groups C and D) was statistically significant. Therefore, we can conclude that freezing-modulated-crosslinking at an object temperature of -80°C and a crosslinker bath temperature of -0.05°C produces printed objects that most closely resemble the size of the intended objects.

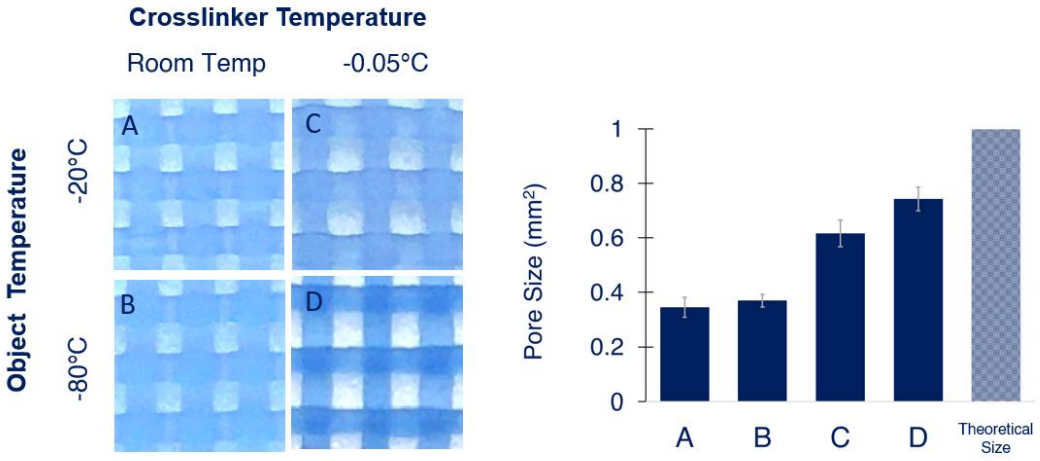

Figure 3.5 3D Cryoprinted lattices crosslinked under various thermal conditions. Average pore size was calculated in ImageJ and compiled in the bar graph. Error bars represent +/- one standard deviation from the mean.

In addition to displaying shrinkage, objects crosslinked at faster melting temperatures displayed a "bulging" effect, as shown by the ring in Figure 3.11A. As stated earlier, the objective of freezing-modulated-crosslinking is to melt the object layer by layer, so that the rigidity of the frozen layer is quickly replaced by rigidity from crosslinking and the object does not change its shape. Based on the mathematical model, we hypothesize that at a faster melting rate the melting interface moves faster than the crosslinking interface, leaving an area of thawed but not yet crosslinked alginate. This soft, thawed area is distorted by the surface tension of the crosslinker bath, creating a "bulged"

shape. To counteract the increased effect of surface tension on the printed objects at cold temperatures, a 5% concentration of Pluronic™ F-68 Non-ionic Surfactant was added to the crosslinking solution for each test. Figure 3.11A demonstrates both the shrinkage effects and the bulging effects that result at faster melting rates. In Figure 3.11C, objects were allowed to thaw completely before crosslinking, and as a result lost their printed structure completely, demonstrating the need for crosslinking during the melting process rather than after.

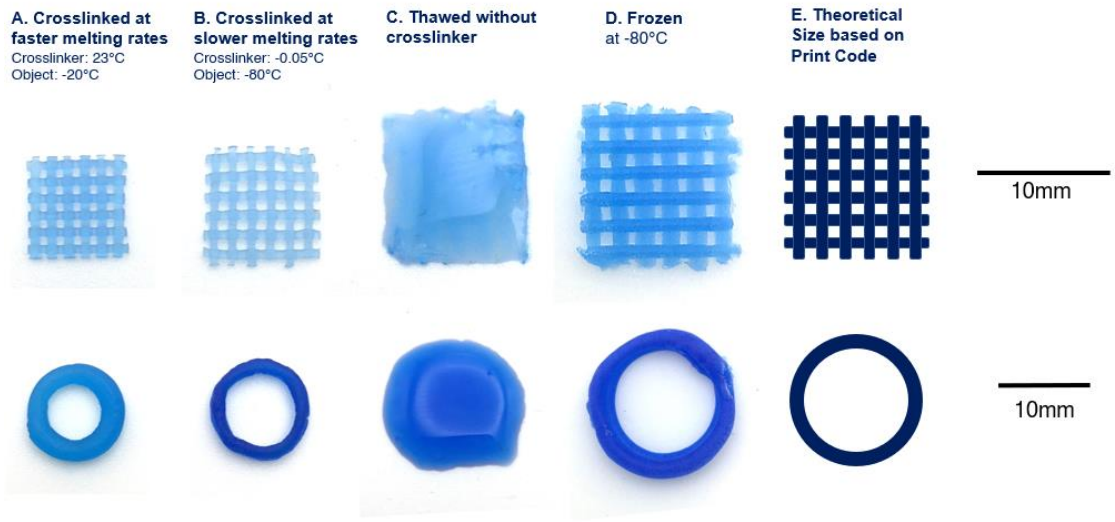

Figure 3.6 3D cryoprinted objects crosslinked with various thermal parameters.

As demonstrated by Figure 3.10 and Figure 3.11, objects that were crosslinked at a slower melting rate most closely resembled the intended printed object. While using freezing-modulated-crosslinking at even slower melting rates was possible, such as with a crosslinker temperature of -2°C, this increased the crosslinking timeframe and there were no noticeable improvements in object accuracy. Thus, an initial object temperature of -80°C and a crosslinker bath temperature of -0.05°C were considered the recommended parameters for freezing-modulated-crosslinking of alginate objects in $CaCl_2$.

3.5.2 Optimizing $CaCl_2$ Concentration

To further characterize the process of freezing-modulated-crosslinking, objects were crosslinked in various concentrations of $CaCl_2$, including 2%, 4%, and 6%. To quantify the amount of shrinkage, the size of the lattice's pores were measured in ImageJ. Based on the results of the thermal parameter testing, an object temperature of -80°C and a crosslinker bath temperature of -0.05°C were used.

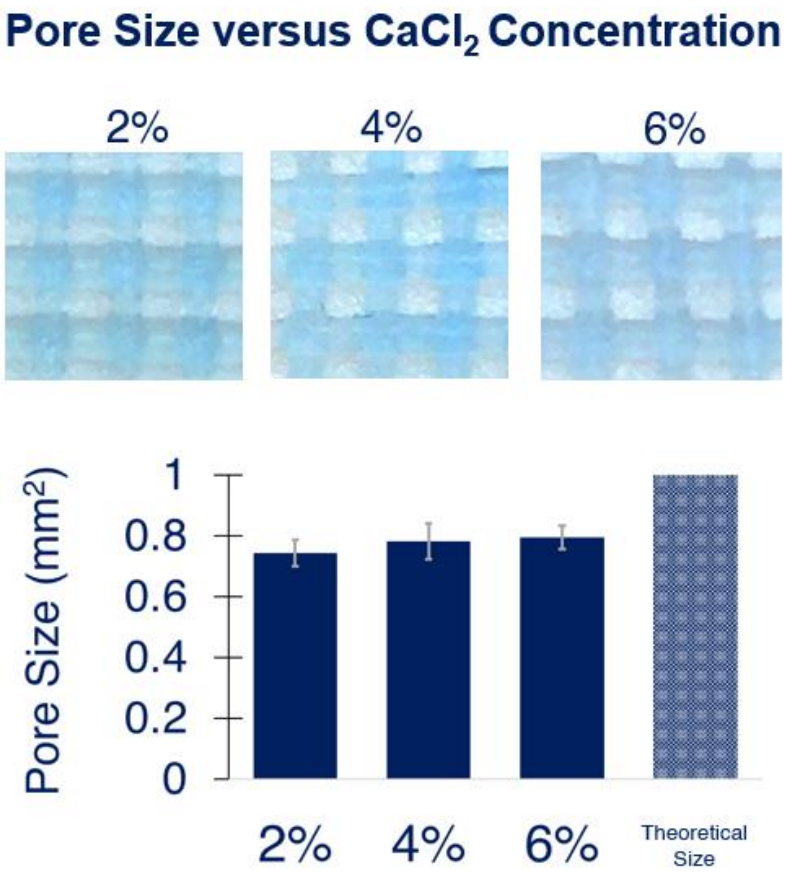

Figure 3.7 3D cryoprinted lattices crosslinked in baths with various concentrations of $CaCl_2$. The difference in pore size between concentrations of $CaCl_2$ was not statistically significant. Error bars represent +/- one standard deviation from the mean.

Whether 2%, 4%, or 6% $CaCl_2$ was used in the crosslinker bath, the lattices displayed the same amount of shrinkage. The difference in pore size for lattices crosslinked with different concentrations of $CaCl_2$ was not statistically significant. This result aligns with our prediction from the mathematical model that at slower melting rates the crosslinking interface will propagate more quickly than the melting interface, so that the limiting rate will be that of the melting interface. In this case, the concentration of Ca^+ ions is unlikely to impact the shape of the object as there will not be areas of un-thawed and un-crosslinked alginate that will be distorted by surface tension. Our experimental results suggest that the concentration of $CaCl_2$ does not impact the size or shape of an object crosslinked with freezing-modulated-crosslinking.

3.5.3 Sample Printed Objects

After determining the optimal crosslinker concentration and thermal parameters for freezing-modulated-crosslinking, the applications of this method were demonstrated by 3D cryoprinting and crosslinking various multi-layer objects. (See Figure 3.13). The following objects were crosslinked at an object temperature of -80°C, a crosslinker bath temperature of -0.05°C, and a $CaCl_2$ concentration of 2%.

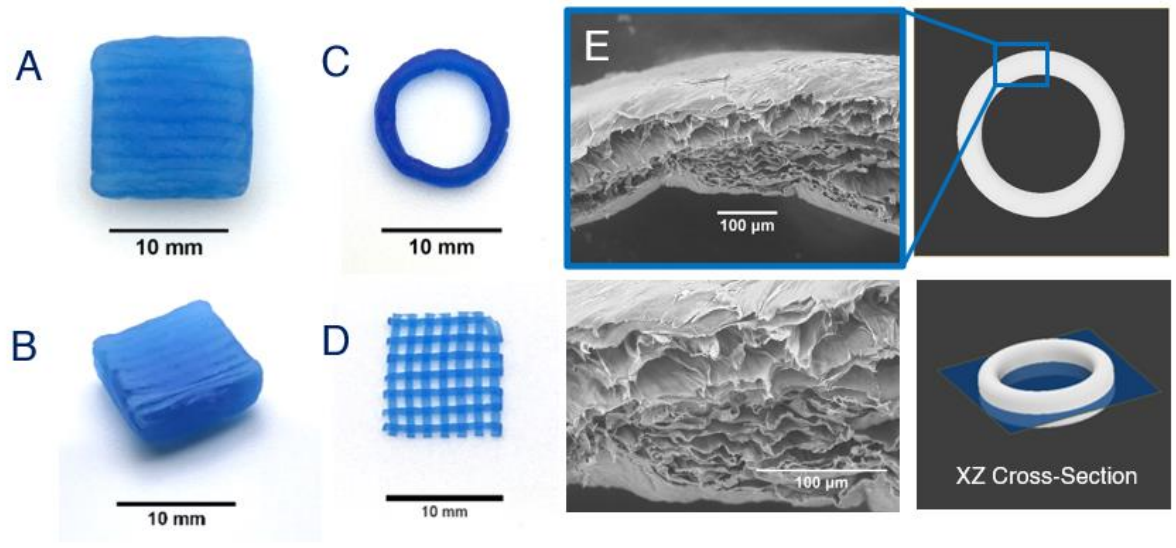

Figure 3.8 Objects printed with 3D cryoprinting and crosslinked by freezing-modulated-crosslinking. A-B) A 3D cryoprinted Cube. C) A 3D cryoprinted Ring. D. A 3D cryoprinted Lattice. E) SEM images of a 3D cryoprinted ring, obtained with an XZ Cross-section.

Multi-layer objects such as the cube and the ring are difficult to fabricate out of soft bioinks without collapse, as are objects with fine details such as the lattice. To demonstrate the porosity of the scaffolds, SEM images were taken of XZ cross-sections of the 3D cryoprinted rings (See Figure 3.13E). The SEM images confirmed that 3D cryoprinting creates highly porous objects with directional pores. The pores here are oriented in the Z-direction, as the ice crystals grow upwards from the chilled print plate. Directional pore networks are advantageous for tissue engineering, as they encourage directional cell growth and result in faster diffusion for drug delivery [89-91]. Our previous work demonstrated that by controlling the freezing speed during 3D cryoprinting it is possible control the shape and size of the pores produced in sodium alginate scaffolds [75].

3.6 Conclusion

Chapter 3 introduced freezing-modulated-crosslinking as a method of crosslinking 3D cryoprinted objects and used a mathematical model to identify the important thermal parameters. The experimental results demonstrated that this method can be used to crosslink objects printed out of soft bioinks without the objects losing their intended shape. An object temperature of -80°C, and a crosslinker bath temperature of -0.05°C produced objects that most closely resembled the intended results. The concentration of $CaCl_2$ in the crosslinker bath did not have a statistically significant impact on the size or shape of the objects. This examination of freezing-modulated-crosslinking expands the possibilities for crosslinking objects produced by 3D cryoprinting.

Chapter 4

4. Maximizing Cell Viability during Temperature-Controlled-Cryoprinting

4.1 Introduction

In Chapter 4, we used Temperature-Controlled-Cryoprinting as a streamlined method of both fabricating and cryopreserving cell-laden 3D scaffolds. We show that Vero cells in a 3D bioprinted scaffold can survive cryopreservation with a viability of 71%, and that cell viability does not decrease as higher layers are printed. Previous methods had either low cell viability or decreasing efficacy for tall or thick scaffolds. We develop an optimal temperature profile for freezing during 3D printing and evaluate drops in cell viability during the various stages of Temperature-Controlled-Cryoprinting.

Historically, cryopreservation has been the main approach for creating stores of cells, tissue constructs, and even whole organs. Cell-laden 3D scaffolds could be cryopreserved, shipped to laboratories, and when ready to be used, thawed, and used for 3D cell culture (See Figure 3.1b). Such a process would dramatically reduce the time and labor associated with 3D scaffolds, hastening the adoption of 3D cell culture. However, the ubiquitous methods used to cryopreserve cells in medium are often ineffective for 3D bioprinted scaffolds. There exists a significant gap in the literature when it comes to cryopreserving cell-laden 3D scaffolds, and current approaches have had limited success [29]. The logical approach seems to be to first 3D bioprint a cell-laden scaffold, and then later freeze it, however there are two major issues with this approach [35]. The first issue is that freezing from outside inward creates an uneven temperature gradient throughout the scaffold such that the cells are frozen at different rates [45]. But in order for cells to survive cryopreservation they must be cooled at very particular rates, such as -1°C/minute. The second problem is the non-uniform distribution of cryoprotectant [35]. Cells deep in the scaffold risk being exposed to insufficient levels of cryoprotectant, and cells at the surface of the scaffold risk death from cryoprotectant toxicity. Both of these issues become magnified the larger the size of the scaffold. Although there have been some successes cryopreserving tissue engineered scaffolds, cell viability is often below 50% and the size of the scaffolds often less than $0.15cm^3$ [35].

Rather than freezing a finished scaffold, a more promising approach is to combine the two steps of 3D printing and cryopreservation into one step, a method known as "3D Cryoprinting". “3D cryoprinting”, also referred to as “3D cryobioprinting,” or “low-temperature 3D bioprinting,” has been used by Ravanbakhsh et al to cryopreserve cell-laden scaffolds for up to three months [47]. Luo et al used cryoprinting to print freestanding filamentous constructs that mimicked the

muscle tendon unit, and Lee et al used cryoprinting to cryopreserve preosteoblasts (MC3T3-E1) [47,46,45]. These approaches can be classified as "static" cryoprinting, as they involve printing onto a static freezing plate, with the nozzle moving upward after each layer (See Figure 4.1a). A notable limitation of static cryoprinting is that as each layer is printed, the nozzle moves further away from the freezing plate and so the temperature at the nozzle rises. As noted by Ravanbakhsh et al., 2022, the reduced heat transfer rate as printing continues prevents the printing of thick constructs and leads to cell death in higher layers [47].

To overcome the issues with static cryoprinting, in Chapter 3 we developed "Temperature-Controlled-Cryoprinting." and used it to fabricate 3D shapes out of alginate, In Chapter 3 we also developed a crosslinking technique called freezing-modulated-crosslinking to crosslink the objects as they thawed [48]. In addition, we demonstrated that the freezing process does not significantly decrease the mechanical strength of 3D scaffolds, but does create interconnected pores [75]. Previously, Temperature-Controlled-Cryoprinting has been used exclusively to fabricate a-cellular scaffolds, but in this study, we demonstrate that it can be used as a method of cryopreserving cell-laden scaffolds. We find that Vero cells in an alginate-collagen bioink can survive Temperature-Controlled-Cryoprinting with a viability of 71% in multi-layer scaffolds. Additionally, we find that cell viability does not decrease as higher layers are printed, demonstrating the merits of Temperature-Controlled-Cryoprinting. Vero cells were used as a test bed because of their widespread use as a host for studying viruses [92]. An effective cryopreservation process for 3D scaffolds laden with Vero cells would allow virology researchers to create a stockpile of cryopreserved scaffolds that could be thawed at any time and infected with a virus. By reducing the time and labor involved with using 3D scaffolds, temperature-controlled cryoprinting could thus remove the barriers to adopting 3D cell culture.

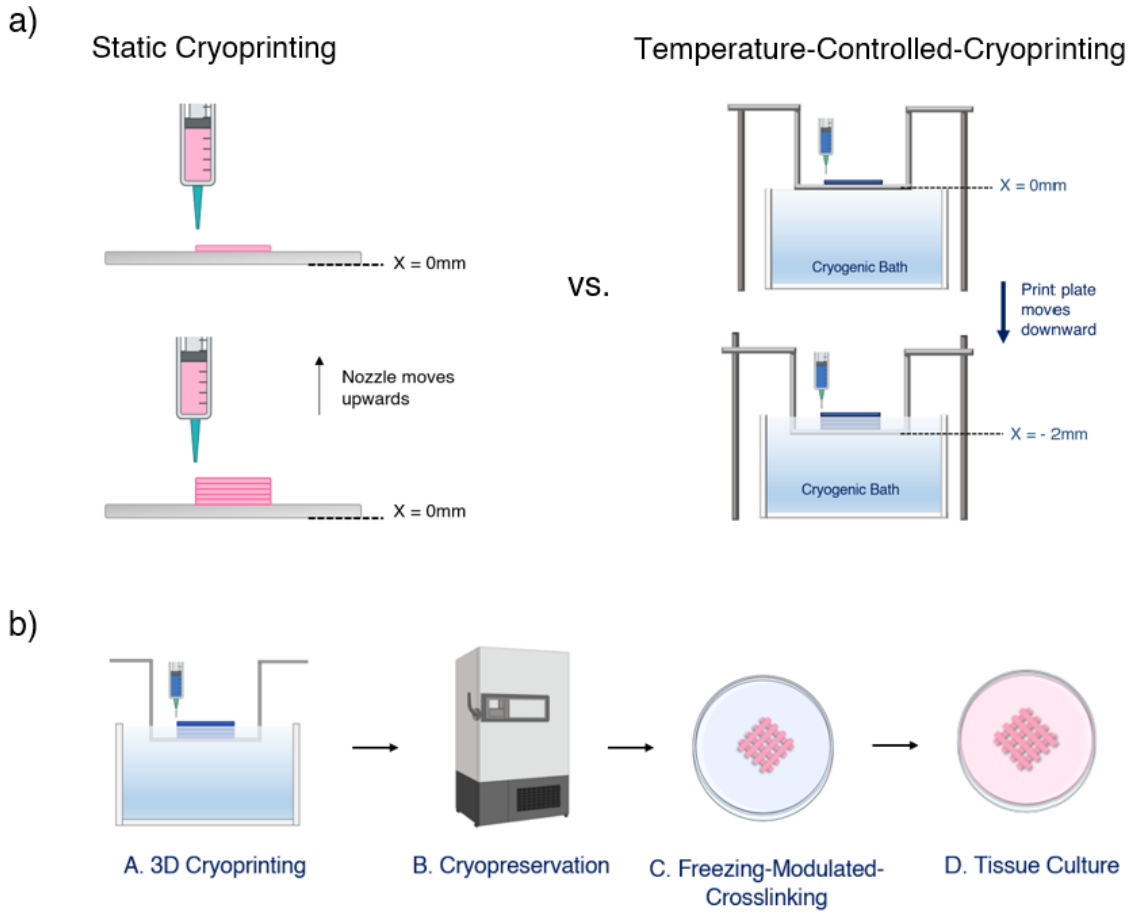

Figure 4.1 A) Static cryoprinting versus Temperature-Controlled-Cryoprinting. B) A supply chain of cell-laden scaffolds from fabrication to use.

4.2. Materials and Methods

4.2.1 Cell Culture

Vero cells were acquired from the University of California-Berkeley Cell Culture Facility and were cultured in 5.0% CO2 at 37.0°C. The cells were grown in DMEM (Gibco) supplemented with 10% heat-inactivated fetal bovine serum (FBS, Life Technologies) and 1% PenStrep (Gibco).

4.2.1 Bioink Preparation

2% (w/v) alginate was made by dissolving sodium alginate (Spectrum Chemical MFG Corp) in DMEM. 1mL of 2% sodium was mixed with 100ul of PureCol® EZ Gel Collagen (Advanced Biomatrix), 100ul of DMSO (Sigma Aldrich), and 300ul of cells suspended in Fetal Bovine Serum at 0.5e6 cells/ml to create a 1% alginate bioink with 10% DMSO and 0.5e6 cells/mL. The bioink was mixed using two syringes and a luer lock coupler at temperatures of either 25°C or 4°C. The bionk was then used directly after or cooled to 0°C.

4.2.2 Temperature-Controlled-Cryoprinting

3D Scaffolds were printed using a custom-modified temperature-controlled-cryoprinter which has been described in detail in previous works [48]. The cooling bath of the temperature-controlled-cryoprinter contained a 45% ethylene-glycol and water solution that was circulated with a Neslab RTE-140 Refrigerated Circulator (Thermo Scientific). During 3D printing, the bioink was extruded through an 18-gauge conical nozzle (Sanants) onto the cooled printing plate which then descended further into the cooling bath by the height of the printed layer. The print plate temperature was kept at -5°C and a printing speed of 2mm/s was used to print 10mm lines (See Figure 4.2.). Some 3D scaffolds were then cooled at -1°C/min to -80°C in a custom, alcohol-based cooling container in a -80°C refrigerator. Others were thawed and crosslinked immediately after printing onto the -5°C plate.

4.2.3 Crosslinking, Thawing and Cryoprotectant Removal

0.5% (w/v) $CaCl_2$ crosslinker was made by dissolving $CaCl_2$ dihydrate powder (Fisher Scientific) in DMEM. The solution was mixed to homogeneity using a magnetic stir plate. Crosslinker was added at different stages based on the experiment, either directly after 3D printing or after cryopreservation at -80°C (See Figure 4.2) Crosslinker at 37°C was poured over the printed objects and left for 1 minute. Then, the crosslinker was removed and the scaffolds were washed three times with DPBS (Sigma Aldrich) to remove excess Ca^{+} ions and to dilute the DMSO in the bioink. Scaffolds containing DMSO were then submerged in cell medium and kept at 4°C for 9 minutes to allow the DMSO to further diffuse out of the scaffolds. The cell medium was then changed, and the scaffolds placed in the incubator. The cell medium was changed again at the one hour and two-hour mark to remove residual DMSO.

4.2.4 Cell Viability Assay

Cells were cultured for 24 hours after each experiment as cell death pathways during cryopreservation take 6-24 hours to complete [38]. Cell viability assays done before this 24-hour period can thus lead to false positive results. Hoechst/Propidium iodide staining was used to assess cell viability according to the manufacturer's protocol (Sigma Aldrich). The cell medium was replaced with DPBS, as well as 1µl/mL Hoechst, and 10µl/mL PI. The scaffolds were incubated at 37°C, 5% CO_2 for 50 minutes, and then imaged with a Nikon Eclipse TE300 inverted microscope (Nikon).

4.2.5 Statistical Analysis

All experiments were done at least in triplicate, and data was presented with ± the standard deviation. A one-way ANOVA was used to compare the means with a Tukey's post hoc test. P-values of 0.05 and 0.01 were used as the thresholds.

4.3 Results

4.3.1 Printing Multi-Layer Scaffolds

We used the temperature-controlled-cryoprinter described previously to print Vero cells encapsulated in an alginate-collagen bioink [48]. Alginate is a popular choice for 3D bioprinting because of its low cost and biocompatibility [62]. In addition, alginate is often used to encapsulate cells for cryopreservation and has demonstrated cryoprotective effects as it reduces ice crystal formation [93]. Alginate was therefore an ideal choice for Temperature-Controlled-Cryoprinting, which combines bioprinting and cryopreservation. Since alginate lacks the adhesion sites necessary for cell proliferation, collagen was added to the bioink in a 10:1 ratio.

Temperature-Controlled-Cryoprinting is a promising cryopreservation method for 3D bioprinted scaffolds because each voxel (volume pixel) of bioink is printed under the same thermal conditions. To demonstrate this effect, thermal images of the nozzle were taken during the first layer and fifth layer of a printed scaffold (See Figure 4.2a). The level of the cooling fluid was such that after three layers were printed the print plate descended and the first layer became submerged in the clear cooling fluid. The three-layer gap prevented the nozzle from touching the cooling fluid and thus freezing and clogging. As demonstrated in Figure 4.2a, the temperature at the nozzle was maintained even as higher layers were printed. Temperature-Controlled-Cryoprinting was used to print an eight-layer line (Figure 4.2b.) and an eight-layer hollow square (Figure 4.2c.) After printing, the scaffolds were thawed and crosslinked in a $CaCl_2$ bath in a process we previously named "freezing-modulated-crosslinking" [48].

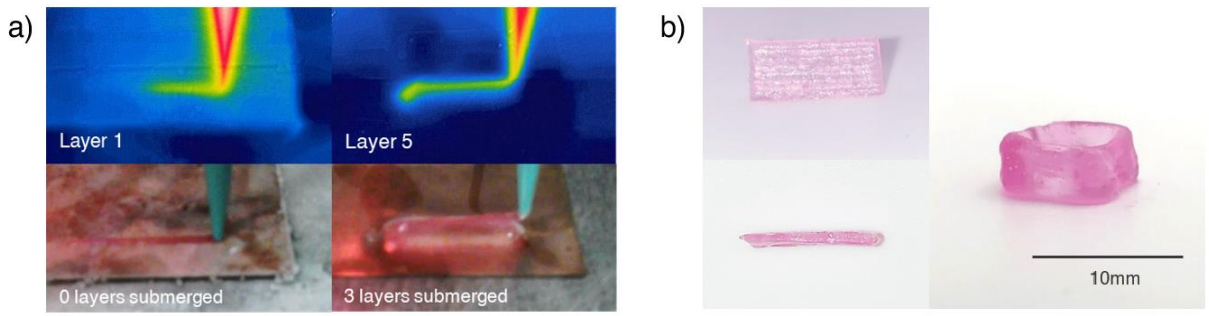

Figure 4.2 Multi-layer scaffolds printed with Temperature-Controlled-Cryoprinting. A) The temperature distribution at the nozzle is constant at the first layer and higher layers B) An eight-layer line and an eight-layer hollow square printed with Temperature-Controlled-Cryoprinting

4.3.2 Cell Viability during Temperature-Controlled-Cryoprinting

The established protocol for cryopreserving mammalian cells is to suspend them in a medium containing 10% DMSO as a cryoprotectant and to slow cool them at -1°C/min until they reach temperatures of lower than -60°C degrees [94, 95]. Extensive research during the past fifty years has affirmed the efficacy of slow cooling at -1°C/min for various mammalian cell types. Although considered the gold standard cryoprotectant, DMSO is toxic to cells at room temperature and so the exposure time should be limited. Ravanbaksch et al found that cells encapsulated in a GelMA bioink experienced significant cell death after 30 minutes of exposure to 10% DMSO [47]. Death from DMSO toxicity can be reduced by exposing it to the cells at 4°C instead of at room temperature, as DMSO is less toxic at lower temperatures. For long term cryopreservation, cells cooled to -80°C should then be cooled to -140°C using liquid nitrogen. However, studies have demonstrated that for short-term storage, the difference between storing cells at -80°C and -140°C is negligible, so for the purpose of this study the 3D bioprinted scaffolds were stored in a -80°C freezer for 24 hours [97, 98]. Future work should study long-term cryopreservation of cryoprinted scaffolds on a timescale of weeks or months.

4.3.3 Effect of Cooling Rate during 3D Printing

Vero cells were mixed into the alginate-collagen bioink with 10% DMSO using two syringes and a luer-lock coupler. Ideally, the cells encapsulated in the bioink and 3D cryoprinted could be cooled at -1°C/minute from room temperature to -80°C. However, the printing step of Temperature-Controlled-Cryoprinting presented some limitations (See Figure 4.3a). The freezing point of the bioink was -5°C and therefore the print plate needed to remain at -5°C or lower for cryoprinting to occur. Lee et al and Ravanbaksch et al found that using print plate temperatures lower than -5°C during static cryoprinting reduced cell viability, likely because the cooling rate from the nozzle temperature to the print plate was too rapid [47, 45]. For the purpose of this study we therefore limited our focus to a print plate temperature of -5°C. A notable feature of this process is that the cells are held at -5°C until the printing process is completed. Within cryopreservation literature this is referred to as a “two-step” freezing protocol. Typically, during two-step freezing the samples are cooled to an initial subzero temperature, held at that temperature for a duration, and then cooled down further to the storage temperature [99]. Higgins et al used two-step freezing with a hold temperature of -5°C to cryopreserve rat embryonic neural cells, and Nsabimana et al used two-step freezing to increase the survival rate of cryopreserved rumen protozoa [100, 101].

To reduce the cooling rate of the bionk closer to -1°C/min during the printing process, the temperature of the bioink in the nozzle could be lowered, for example to 4°C (See Figure 4.3b). However, lowering the temperature of the bioink increases the viscosity and there becomes an increased risk of cell death from shear stress as the bioink is extruded through the nozzle. Preventing cell death from shear stress is a particular challenge for extrusion-based 3D printing [102]. To test the impact of the bioink temperature in the nozzle, we compared the cell viability for bioinks that were cooled to either 25°C, 4°C, or 0°C, and then extruded onto a -5°C print plate (See Figure 4.3c). Cell death was predicted to be lower when the bioink nozzle temperature was lower because 1) DMSO is less toxic to cells at lower temperatures and 2) The cells were cooled at a slower rate during the 3D printing process. As shown by Figure 4.3c, cooling the bioink to 0°C before 3D cryoprinting resulted in the highest cell viability of 83.8% ± 7.19, while cooling the bioink to 4°C resulted in a cell viability of 77.9% ± 8.54, and a bioink temperature of 25°C resulted in a cell viability of 73.2% ± 6.01. A one-way ANOVA with a Tukey's post hoc test found that the drop in cell viability between the bioink cooled to 0°C and the bioink at 25°C was statistically significant.

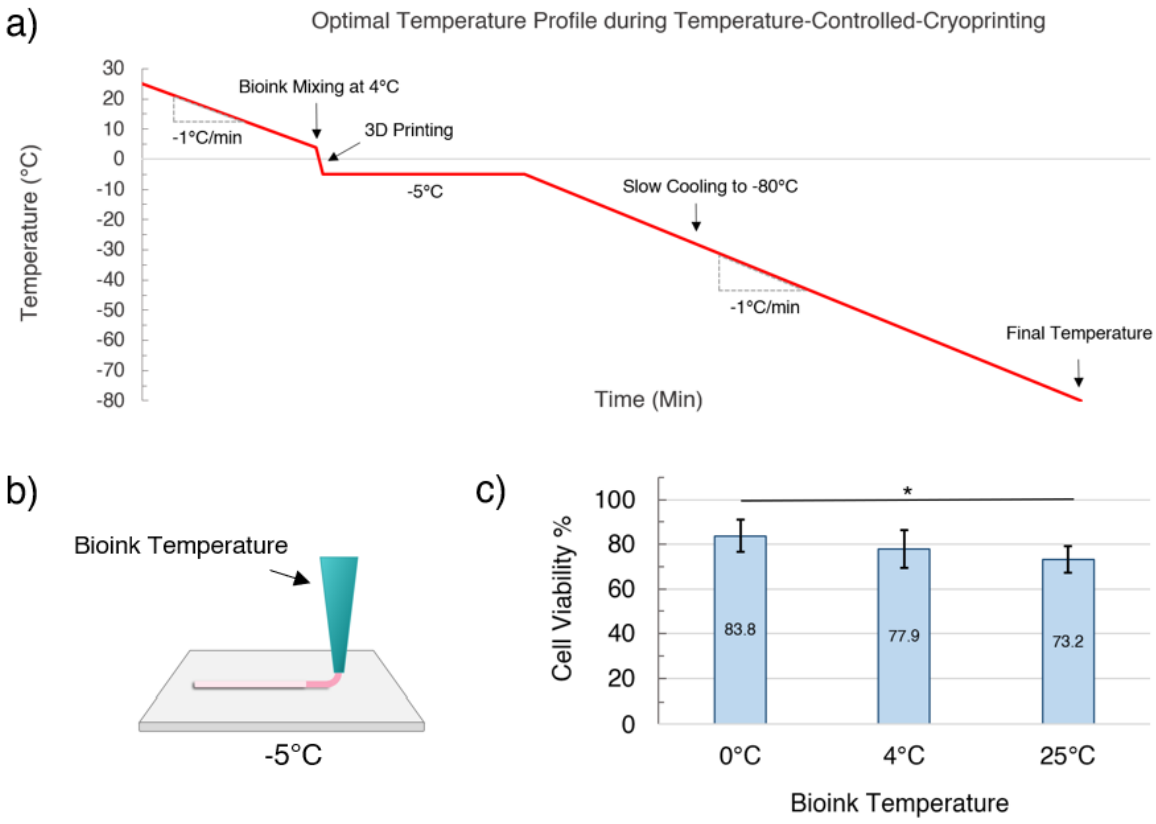

Figure 4.3 A) An optimal temperature profile for Temperature-Controlled-Cryoprinting and subsequent cooling to -80°C B) Initial bioink temperature and extrusion onto a -5°C print plate during Temperature-Controlled-Cryoprinting C) Cell viability rates versus initial bioink

temperature. *p < 0.05, **p < 0.01 and error bars represent ± one standard deviation from the mean.

4.3.4 Cell viability by Layer

A key facet of temperature-controlled cryoprinting is the ability to print multiple layers under the same thermal conditions. Previous literature reported cell viabilities in scaffolds up to three layers [45, 47]. Using static cryoprinting, printing higher layers either became impossible because the bioink no longer froze or undesirable because cell viability decreased. Because the print plate descends further into the cooling bath as each layer is printed, Temperature-Controlled-Cryoprinting presents a method of printing higher layers without compromising cell viability. We compared cell viability between the first and fifth layer for five-layer scaffolds that were cryoprinted and then cooled to -80°C (see Figure 4.4). Cells were stained with Hoechst and Propidum Iodide, which stained all cells blue and dead cells red. A one-way ANOVA with a Tukey's post hoc test was used to assess statistical significance. The average cell viability for Layer 1 was 71.56% ± 8.36 and for Layer 5 was 71.73% ± 6.45. There was no statistically significant difference in cell viability between the layers with p-value of 0.963. Therefore, we conclude that printing higher layers did not compromise cell viability. Within the field of cryopreservation, cell viability above 70% is generally considered a success [35].

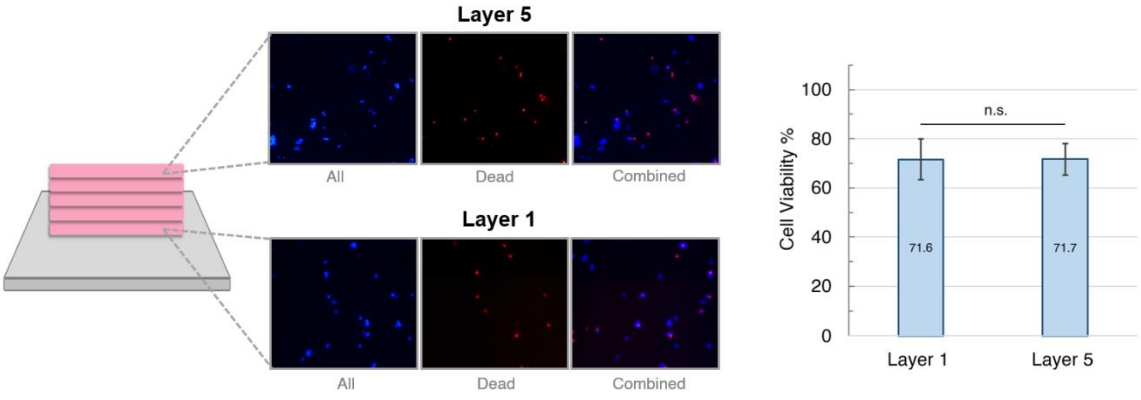

Figure 4.4 A comparison of cell viability in the first and fifth layers of five-layer scaffolds printed at -5°C and cryopreserved at -80°C. Fluorescence images include all cells (blue) and dead cells (red). The p-value was and 0.963 and error bars represent ± one standard deviation from the mean.

4.3.5 Maximizing cell viability during the stages of 3D cryoprinting

To further elucidate which stages of Temperature-Controlled-Cryoprinting caused cell death, we assessed cell viability in one-layer scaffolds after the completion of each step (Figure 4.4.) During the control trial, the cells were mixed into a bioink at room temperature and extruded through the nozzle onto a room temperature plate. They were then crosslinked, washed, and cultured for 24 hours. Average cell viability after the control trial was 87.13% ± 4.51, which is reasonable for 3D bioprinting, suggesting that the process of bioink mixing, extrusion through the nozzle, and crosslinking caused minimal cell death. During the control with DMSO trial, the cells were mixed into a bioink containing 10% DMSO at room temperature. The bioink was then extruded through a nozzle onto a room temperature plate, crosslinked, washed, and cultured for 24 hours. The difference in cell viability between the control trial and the control with DMSO trial was not statistically significant, which suggests that exposure to DMSO at room temperature during the bioink mixing and crosslinking stages did not cause significant cell death. This further suggests that the higher cell viability obtained in Figure 4.3c for bioink cooled to 0°C before printing was due to the slower cooling rate rather than the reduced exposure to DMSO. During the 3D cryoprinting trial, the cells were cooled to 4°C and then mixed into a 4°C bioink containing 10% DMSO. The bioink was then cooled to 0°C before being 3D printed onto a -5°C plate. The 3D scaffold was then crosslinked, washed, and cultured for 24 hours. The average cell viability for this trial was 83.76% ± 7.19, which was not a statistically significant difference from the two control trials. During the 3D cryoprinting and cooling to -80°C trial, the cells were cooled to 4°C and then mixed into a 4°C bioink containing 10% DMSO. The bioink was then cooled to 0°C before being 3D printed onto a -5°C plate and then the scaffold was cooled at -1°C/minute to -80°C. 24 hours later, the scaffold was thawed in a 37°C crosslinker bath, washed, and then cultured for 24 hours. The average cell viability was 71.83% ± 7.41, which was a statistically significant drop from the 3D cryoprinting trial. The result of this experiment suggests that the largest drop in cell viability during Temperature-Controlled-Cryoprinting occurs as a result of the cells being cooled from -5°C to -80°C. This is not unexpected, as the most lethal temperature zone to cells during cryopreservation is between -15°C to -60°C [41]. The cells traverse this temperature zone twice, once while slow cooling to -80°C at -1°C/min and a second time while thawing. Within this temperature zone, ice first forms outside of the cell membrane, increasing the solute concentration and causing osmotic shock. As the temperature continues to lower, intracellular ice forms which penetrates the cell membrane, leading to cell death [41]. This two-factor mechanism of cell death can be reduced with an optimized composition of cryoprotectants and post-thawing additives. Therefore, cell viability of greater than 71% during Temperature-Controlled-Cryoprinting could likely be achieved with further research. In addition, the bioink composition can also be optimized to achieve cell viability of higher than 87% in the control trials.

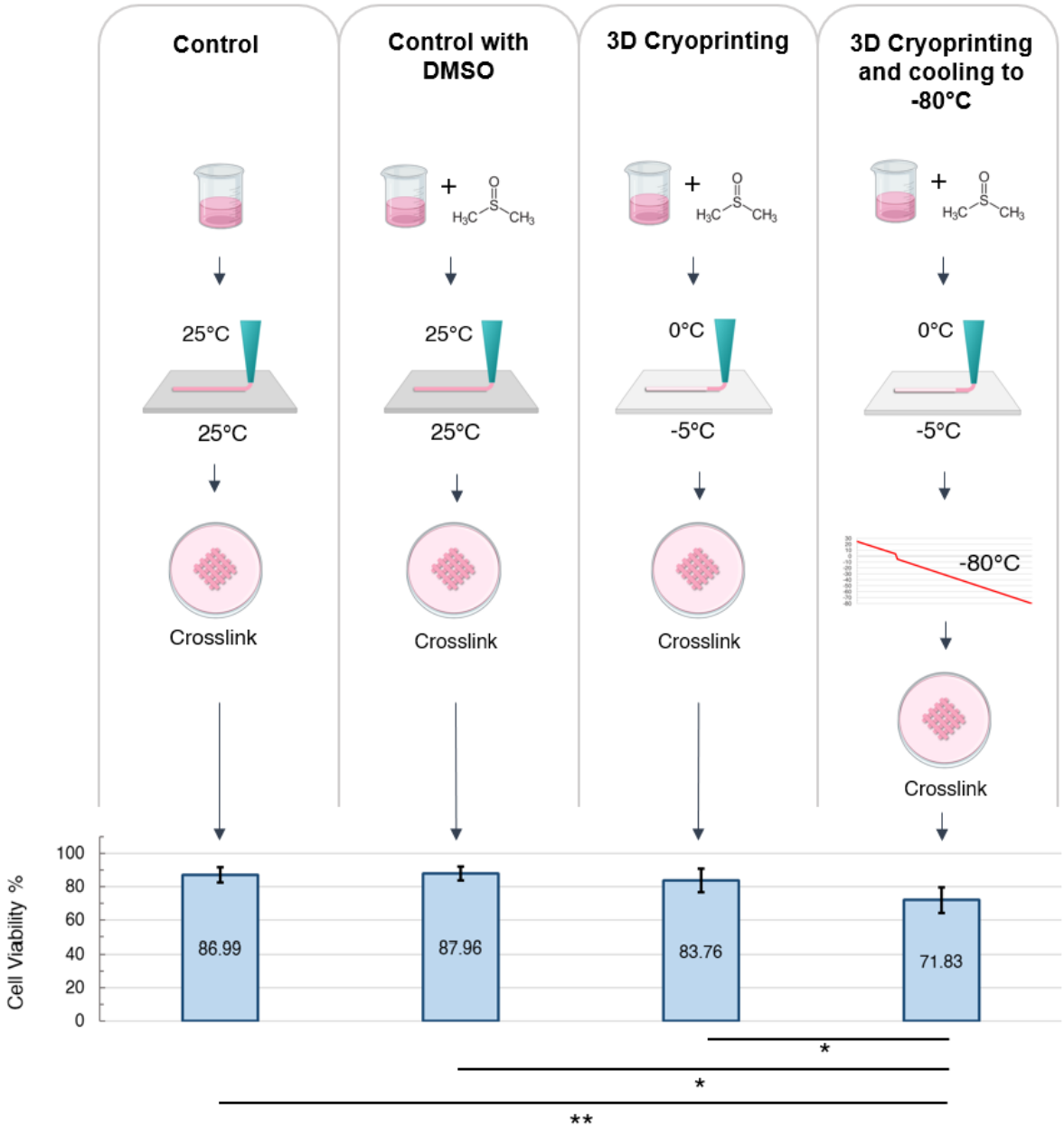

Figure 4.5 Assessing cell viability during the different stages of the Temperature-Controlled-Cryoprinting process. *p<0.05, **p<0.01 and error bars represent ± one standard deviation from the mean.

4.4 Conclusion

In summary, Chapter 4 investigated the use of Temperature-Controlled-Cryoprinting as a method of fabricating and cryopreserving 3D bioprinted scaffolds. 3D bioprinted scaffolds are far better at mimicking the 3D tissue microenvironment than 2D cell culture, and expanded use of 3D bioprinted scaffolds could speed up drug discovery [2]. The availability of cryopreserved Vero cells in 3D scaffolds would allow virology researchers to create a stockpile of scaffolds for studying new viruses and allow labs without 3D bioprinting resources to receive shipments of cell-laden scaffolds from across the world.

We found that Temperature-Controlled-Cryoprinting could be used to fabricate and cryopreserve 3D bioprinted scaffolds with an average cell viability of 71.64% ± 7.47. Higher cell viability could likely be achieved by optimizing the bioink composition and the cryoprotectant composition. For example, the use of commercial cryopreservation mediums such as CryoStor® or Unisol™ or the addition of saccharides in the cryopreservation medium have all been shown to significantly increase cell viability after cryopreservation [103, 47]. The use of post-thaw additives such as free radical scavengers/antioxidants has also been shown to significantly increase cell viability in cryopreserved cells [104].

We found that printing with an initial bioink temperature of 0°C onto a printing plate at -5°C resulted in a higher cell viability than using a bioink temperature of 4°C or 25°C, and our experiments suggested that this was due to the slower cooling rate during printing. Surprisingly, cell exposure to DMSO during Temperature-Controlled-Cryoprinting did not pose an issue, but further work could also study the impact of reducing DMSO concentration. Most notably, Temperature-Controlled-Cryoprinting was used in this study to print higher layers than has been achieved with static cryoprinting, cell death did not increase as higher layers were printed. Temperature-controlled cryoprinting thus solves an important limitation of static cryoprinting, which is that the cooling rate decreases as further layers are printed and become further away from the print plate. Further studies could investigate the use of Temperature-Controlled-Cryoprinting for fabricating large-volume scaffolds and even higher layers. In conclusion, Temperature-Controlled-Cryoprinting is a promising fabrication and cryopreservation technique for 3D bioprinted scaffolds that could expand access to 3D cell culture.

5. Conclusion

2D cell culture has been the dominant method of modeling the human body for hundreds of years, despite evidence that cells in 2D respond differently than cells grown in a 3D environment such as the body. While 2D cell culture is simple, efficient, and cheap to use, the past twenty years have ushered in many promising alternatives, which fall under the umbrella of "3D cell culture." Interest in organoids, organs-on-a-chip, and 3D bioprinted scaffolds is growing rapidly. 3D cell culture is particularly promising for the drug development industry, as the use of 2D cell culture is a known issue that contributes to the high failure rate of new drugs. Drug development is a costly endeavor, as it can take upwards of ten years and close to 2 billion dollars to bring a new drug to market. Unfortunately, the industry is stymied by a high rate of failure during the later stage of development. 2D cell culture is heavily relied upon during the earlier stages, despite evidence that cells in 2D are a poor predictor of results in humans. Many drugs that appear effective in 2D cultures later have low efficacy in clinical trials. The early 2000's ushered in many new technologies for fabricating 3D cell culture, and 3D bioprinting in particular offers unprecedented control over the microarchitecture of the scaffold and the placement of multiple cell types. But the transition from 2D cell culture to 3D bioprinted scaffolds requires a "scaling-up" of production that 3D bioprinting has not yet achieved. One key aspect of this "scaling-up" is the ability to cryopreserve 3D bioprinted scaffolds. Cryopreservation is a fundamental process for the use of biological material. Without the ability to cryopreserve cell lines for weeks to years, many cell lines would no longer be available. Cells in continuous culture experience genetic changes over time, and so cryopreservation is a vital tool for maintaining cell lines and preserving genetic characteristics. Logistically, the ability to cryopreserve cells saves resources, time, money, and lab space. Cryopreservation is particularly important for the expanded use of 3D bioprinted scaffolds, given the comparatively long lead time for fabrication. Compared to 2D cell culture, fabricating 3D scaffolds is a far more laborious and time-consuming process. Achieving the high-throughput methods that are possible with 2D cell culture is difficult without a method to cryopreserve 3D bioprinted scaffolds. In addition, cryopreservation is crucial for the shipping and transfer of biological material. Shipping 3D bioprinted scaffolds to laboratories that are more than a few hours away is challenging and often impossible for 3D bioprinted scaffolds that are not cryopreserved. Therefore, there is an urgent need to develop methods of cryopreserving 3D bioprinted scaffolds.

Unfortunately, the cryopreservation of 3D bioprinted scaffolds is not as trivial of a process as the cryopreservation of cells suspended in media. The established methods for cryopreserving cells in 2D have not been effective for cryopreserved 3D bioprinted scaffolds. As with organs, tissues, and other biological material, the larger the size of the 3D construct, the more difficult it is to cryopreserve it. Freezing a 3D bioprinted scaffold from the outside inward creates an uneven temperature gradient, which results in cells in different parts of the scaffold being frozen at different rates. As discussed in Chapter 1., the use of particular freezing rates is crucial to achieve cell survival. In addition to this heat transfer issue, there is also a challenge with achieving a uniform distribution of cryoprotectants throughout the scaffold. When cryoprotectants are added outside of a scaffold to be diffused inward, the cells in the middle of the scaffold risk levels of cryoprotectant that are too low to prevent death during freezing, and cells in the outside of the scaffold risk death from cryoprotectant toxicity. This heat transfer and mass transfer issue become

magnified as the volume of the scaffold increases. For this reason, the cryopreservation of 3D bioprinted scaffolds have been mostly limited to scaffolds under a size of $0.15cm^3$.

A new approach to the cryopreservation of 3D bioprinted scaffolds was invented in 2008 by Adamkiewicz et al, and further developed in the 2020's by Lee et al, Ravanbakhsh et al, and Luo et al. This method, termed "3D cryoprinting," or "3D cryobioprinting," involves extruding the bioink onto a freezing plate, such that fabrication and cryopreservation of 3D bioprinted scaffolds is combined into one step. A limitation of previous work with 3D Cryoprinting, is that the bioink was extruded onto a static freezing plate, and thus as higher layers were printed, after a while they failed to freeze. This issue also limited the size of the scaffolds that could be cryopreserved, with researchers only reporting results for scaffolds that were three layers high or less. This thesis presented "Temperature-Controlled-Cryoprinting," as a method of printing onto a dynamic freezing plate. During Temperature-Controlled-Cryoprinting, the freezing plate descends further into a cooling bath with every layer that is printed, keeping the temperature at the nozzle constant. As a result, Temperature-Controlled-Cryoprinting ensures that every cell that is printed in the scaffold is frozen at the same freezing rate. This is key to achieving uniform cell viability and microarchitecture throughout the scaffold. Unlike previous methods, the size of the scaffold is not limited by the printing method.

5.1 Major Findings

This thesis developed Temperature-Controlled-Cryoprinting as a method of cryopreserving 3D bioprinted scaffolds and achieved a high cell viability rate. Chapter 2 investigated the influence of crosslinking order and cooling rate on the microstructure and mechanical properties of single-layer, sodium alginate scaffolds. A novel, modular 3D printer was built in order to study the effects of these steps separately and to address many of the manufacturing issues associated with 3D cryoprinting. The modular 3D printer allowed 3D printing, crosslinking, and freezing to be conducted on separate modules yet remain part of a continuous manufacturing process. Chapter 2 found that crosslinking before the freezing step produced highly interconnected and directional pores, which are ideal for promoting cell growth. The size of the pores could be controlled by controlling the cooling rate. Including freezing in the 3D bioprinting process did not decrease the tensile strength of the scaffolds, although there was a significant loss in firmness for strands with larger pores. In Chapter 3, a novel, Temperature-Controlled-Cryoprinter was presented with the ability to print multi-layer structures under uniform thermal conditions. Then, a process for crosslinking these frozen scaffolds named freezing-modulated-crosslinking was developed to prevent them from collapsing as they thawed. During freezing-modulated-crosslinking, the frozen scaffold is placed into a bath of crosslinker which is held at a particular temperature. Mathematical and experimental results found that by controlling the initial temperature of the scaffold and the temperature of the crosslinker bath, the rate of thawing and the rate of crosslinking can be controlled. In Chapter 3.3, we qualitatively examined the effect of these parameters by printing various shapes out of 2% sodium alginate and crosslinking them in a $CaCl_2$ bath with freezing-modulated-crosslinking. Then, to further characterize freezing-modulated-crosslinking, we examined the impact of $CaCl_2$ concentration and found that it had no impact. These results demonstrated that the rate of crosslinking was indeed being modulated by the rate of freezing. The

experimental section found that an object temperature of -80°C, and a crosslinker bath temperature of -0.05°C produced objects that most closely resembled the intended results. The development of freezing-modulated-crosslinking in Chapter 3 therefore expanded the type of biomaterials that can be used for 3D cryoprinting and the type of structures that can be printed out of soft bioinks.

Finally, Chapter 4 assessed the use of Temperature-Controlled-Cryoprinting to cryopreserve cell-laden scaffolds. The printer developed in Chapter 3 was used to print Vero cells encapsulated in an alginate-collagen bioink [48, 105]. Then, the freezing-modulated-crosslinking process developed in Chapter 3 was used to ionically crosslink the alginate-collagen scaffolds during thawing. Experiments were done in Chapter 4 to maximize cell viability during the various stages of Temperature-Controlled-Cryoprinting. An optimal temperature profile for slow freezing during 3D cryoprinting was developed. Experiments found that using an initial bioink temperature of 0°C resulted in a higher cell viability than using a bioink temperature of 4°C or 25°C, due to the slower cooling rate during printing. Exposure to DMSO during Temperature-Controlled-Cryoprinting did not cause a statistically significant drop in cell viability. Chapter 4 presented the highest number of cryoprinted layers in a scaffold to date, by printing an eight-layer scaffold. Cell death did not increase as higher layers were printed, confirming the advantages of Temperature-Controlled-Cryoprinting as a method of printing large 3D bioprinted scaffolds. This thesis therefore presents a solution to a notable challenge in static cryoprinting, that the freezing rate decreases as layers become further away from the print plate.

5.2 Future Perspectives

This thesis presented the highest number of layers in a cryopreserved 3D bioprinted scaffold to date. However, the full capabilities of Temperature-Controlled-Cryoprinting have not yet been explored. Future work should be done to use Temperature-Controlled-Cryoprinting to cryopreserve 3D bioprinted scaffolds with higher layers and larger volumes. While this thesis has focused on the cryopreservation of 3D bioprinted scaffolds for applications in drug development, the possible applications of Temperature-Controlled-Cryoprinting go much further. Currently, 3D bioprinting is being explored as a method of fabricating scaffolds for tissue transplantation and organ repair. Scaffolds can be printed out of the patient's own cells and transplanted into the patient to repair defects in tissue or organs. One notable success includes the recent transplantation of a 3D bioprinted ear onto a patient who was born with a missing ear [106]. Temperature-Controlled-Cryoprinting offers a few advantages for this application. First, Temperature-Controlled-Cryoprinting could be used to increase the availability of cell-laden scaffolds. For example, every year, thousands of injuries and accidents result in soft tissue injuries that are too large for the patient's body to heal on their own. Cell-laden scaffolds can be transplanted into the patient's body to repair large tissue defects, however the long lead time for fabrication prevents them from being used in emergency procedures [107]. Therefore, there is an urgent need to cryopreserve cell-laden scaffolds so they can be stockpiled and available when needed. Second, Temperature-Controlled-Cryoprinting could protect cells from environmental stressors during the long fabrication time required for large scaffolds. 3D bioprinting researchers hope that 3D bioprinted organs could one day be transplanted into patients in need of an organ replacement. However, bioprinting an organ is a complicated and time-consuming print that would likely take multiple hours. By

cryopreserving the organ as it is being printed, the cells that are extruded in the beginning of the print would be protected from the temperature stressors and lack of nutrients that could cause cell death during extended print times. Therefore, Temperature-Controlled-Cryoprinting could offer advantages to the 3D bioprinted of scaffolds outside of drug development, but future work is necessary to explore these applications.

This thesis demonstrated Temperature-Controlled-Cryoprinting's efficacy as a method of cryopreserving 3D bioprinted scaffolds. Chapter 3 found that cells could be cryopreserved in a multi-layer scaffold with a viability of above 70%. For this proof-of-concept study, 10% DMSO was used as the cryoprotectant due to its ubiquity for the cryopreservation of mammalian cells. However, Chapter 3 did not explore the optimization of the cryoprotectant composition. Likely, an exploration into other cryoprotectant compositions would lead to a higher cell viability within the scaffold. As mentioned in Chapter 1, permeating cryoprotectants like DMSO are often coupled with non-permeating cryoprotectants like disaccharides, which inhibit extracellular ice formation. Ravanbakhsh explored various disaccharides in conjunction with 10% DMSO and found that the use of 12% melezitose improved cell viability rates. Alternatively, commercial cryopreservation mediums such as CryoStor® or Unisol™ have been shown to significantly increase cell viability after cryopreservation [103, 47]. The use of post-thaw additives such as free radical scavengers/antioxidants has also been shown to significantly increase cell viability in cryopreserved cells [106]. Therefore, future work could be done to maximize cell viability during Temperature-Controlled-Cryoprinting by optimizing the cryoprotectant composition. Another remaining avenue of exploration is the use of alternative bioinks. As discussed in Chapter 1, 3D bioprinting uses a variety of biocompatible bioinks, including GelMA, collagen, and Hyaluronic acid. The use of different bioinks would require different crosslinking approaches and would result in a different microarchitecture created after freezing. In addition, different bioinks have different cryoprotective properties. One interesting avenue to explore is the use of polyampholytes in 3D bioprinting, as the cryoprotective properties of polyampholytes have been demonstrated extensively [108].

While 70% viability of Vero cells is considered a success in the context of cryopreservation, certain cells such as primary cells and stem cells are more sensitive to cryopreservation and cryoprotectant exposure. Therefore, the Temperature-Controlled-Cryoprinting process would have to be further optimized to maximize cell viability for these cells. In addition, the work presented in this thesis was limited as it only assessed cell health after 24 hours, and not for subsequent days or weeks. Future work should assess the health of cells in the scaffold on the timescale of weeks. As the 3D bioprinting field has progressed, the complexity of 3D bioprinted scaffolds has increased. Scaffolds with multiple materials and multiple cell types better represent the 3D microenvironment found in the body. Future work with Temperature-Controlled-Cryoprinting should explore the fabrication of scaffolds meant to mimic a particular tissue. One example is the 3D bioprinting of liver constructs. The liver contains many types of cells, including hepatocytes, hepatic stellate cells, endothelial cells Kupffer cells, and epithelial cells [109]. Therefore, a 3D bioprinted construct meant to mimic the liver should have multiple cell types, or contain stem cells that are then differentiated into these cells types. Within the liver, these cell types are arranged in a particular order in a hexagonal block known as the hepatic lobule. Each liver in the human body contains up to one million of these lobules. Therefore, a 3D bioprinted scaffold should have a geometry that mimics the organization of these lobules. The liver is supplied by two blood supply systems, venous blood from the gastrointestinal tract and arterial blood from the systemic

circulation. Therefore, a 3D bioprinted liver scaffold should have a similar vasculature. Temperature-Controlled-Cryoprinting of a liver construct would therefore require a complex design, including multiple materials and cell types, that has not yet been explored.

5.3 Closing Statement

The use of 3D bioprinted scaffolds has many advantages over the use of 2D cell culture for modeling the human body. Extensive evidence has shown that 2D cells act very differently than cells cultured in the 3D microenvironment of the body, particularly in the context of drug testing. The overreliance on 2D cell culture has led to high failure rates and expanding costs for drug development. 3D bioprinted scaffolds offer a far more sophisticated model of the human body, and due to the FDA modernization act, could even replace animal models. However, the use of 3D bioprinting has been held back by the difficulty of cryopreserving 3D bioprinted scaffolds. Freezing a large, 3D scaffold creates an uneven temperature gradient and an unequal distribution of cryoprotectants, which compromises cell viability. This thesis presented "Temperature-Controlled-Cryoprinting" as a method of both fabricating and cryopreserving 3D bioprinted scaffolds. During Temperature-Controlled-Cryoprinting, a cell-laden ink is printed on a freezing plate. As each layer is printed, the print plate descends further into a cooling bath, which ensures that all cells in the scaffold are frozen at the same rate. In Chapter 1 we explored the fundamentals of Temperature-Controlled-Cryoprinting, including the impact that freezing has on the mechanical and material properties of the scaffolds. In Chapter 2 we then discussed the optimization of the 3D printing process, and how to enhance scaffold stability with crosslinking. In Chapter 4 we discussed the use of Temperature-Controlled-Cryoprinting for the cryopreservation of 3D bioprinted scaffolds, and how to maximize cell viability. In conclusion, Temperature-Controlled-Cryoprinting is a promising method of cryopreserving 3D bioprinted scaffolds that could hasten the transition away from 2D cell culture and accelerate medical research.

References

[1] Segeritz, C. P., & Vallier, L. (2017). Cell culture: Growing cells as model systems in vitro. In Basic science methods for clinical researchers (pp. 151-172). Academic Press.

[2] Langhans, S. A. (2018). Three-dimensional in vitro cell culture models in drug discovery and drug repositioning. Frontiers in pharmacology, 9, 334617.

[3] Jensen, C., & Teng, Y. (2020). Is it time to start transitioning from 2D to 3D cell culture?. Frontiers in molecular biosciences, 7, 33.

[4] Hussey, G. S., Dziki, J. L., & Badylak, S. F. (2018). Extracellular matrix-based materials for regenerative medicine. Nature Reviews Materials, 3(7), 159–173.

[5] Joseph, J. S., Malindisa, S. T., & Ntwasa, M. (2018). Two-dimensional (2D) and three-dimensional (3D) cell culturing in drug discovery. *Cell Culture*, *2*, 1-22.

[6] Congressional Budget Office, 2021. "Research and Development in the Pharmaceutical Industry," Reports 57025, Congressional Budget Office.

[7] Foglizzo, V., Cocco, E., & Marchiò, S. (2022). Advanced Cellular Models for Preclinical Drug Testing: From 2D Cultures to Organ-on-a-Chip Technology. Cancers, 14(15), 3692.

[8] Białkowska, K., Komorowski, P., Bryszewska, M., & Miłowska, K. (2020). Spheroids as a type of three-dimensional cell cultures—examples of methods of preparation and the most important application. *International journal of molecular sciences*, *21*(17), 6225.

[9] de Dios-Figueroa, G. T., Aguilera-Marquez, J. D. R., Camacho-Villegas, T. A., & Lugo-Fabres, P. H. (2021). 3d cell culture models in covid-19 times: A review of 3D technologies to understand and accelerate therapeutic drug discovery. *Biomedicines*, *9*(6), 602.

[10] Elemoso, A., Shalunov, G., Balakhovsky, Y. M., Ostrovskiy, A. Y., & Khesuani, Y. D. (2020). 3D Bioprinting: The roller coaster ride to commercialization. *International Journal of Bioprinting*, *6*(3).

[11] Singh, D., Mathur, A., Arora, S., Roy, S., & Mahindroo, N. (2022). Journey of organ on a chip technology and its role in future healthcare scenario. *Applied Surface Science Advances*, *9*, 100246.

[12] Corrò, C., Novellasdemunt, L., & Li, V. S. (2020). A brief history of organoids. *American Journal of Physiology-Cell Physiology*, *319*(1), C151-C165.

[13] Gu, Z., Fu, J., Lin, H., & He, Y. (2020). Development of 3D bioprinting: From printing methods to biomedical applications. Asian Journal of Pharmaceutical Sciences, 15(5), 529-557.

[14] Zushin, P. J. H., Mukherjee, S., & Wu, J. C. (2023). FDA Modernization Act 2.0: transitioning beyond animal models with human cells, organoids, and AI/ML-based approaches. *Journal of Clinical Investigation*, *133*(21), e175824.

[14] Ravanbakhsh, H., Karamzadeh, V., Bao, G., Mongeau, L., Juncker, D., & Zhang, Y. S. (2021). Emerging Technologies in Multi-Material Bioprinting. Advanced Materials, 33(49), 2104730.

[15] Gungor-Ozkerim, P. S., Inci, I., Zhang, Y. S., Khademhosseini, A., & Dokmeci, M. R. (2018). Bioinks for 3D bioprinting: an overview. Biomaterials science, 6(5), 915-946.

[16] GhavamiNejad, A., Ashammakhi, N., Wu, X. Y., & Khademhosseini, A. (2020). Crosslinking Strategies for 3D Bioprinting of Polymeric Hydrogels. Small, 2002931. https://doi.org/10.1002/smll.202002931

[17] Hu, W., Wang, Z., Xiao, Y., Zhang, S., & Wang, J. (2019). Advances in crosslinking strategies of biomedical hydrogels. Biomaterials Science, 7(3), 843–855. https://doi.org/10.1039/c8bm01246f

[18] Knowlton, S., Yenilmez, B., Anand, S., & Tasoglu, S. (2017). Photocrosslinking-based bioprinting: Examining crosslinking schemes. Bioprinting, 5, 10–18. https://doi.org/10.1016/j.bprint.2017.03.001

[19] Ahn, S., Lee, H., Bonassar, L. J., & Kim, G. (2012). Cells (MC3T3-E1)-laden alginate scaffolds fabricated by a modified solid-freeform fabrication process supplemented with an aerosol spraying. Biomacromolecules, 13(9), 2997-3003.

[20] Li, H., Tan, Y. J., Liu, S., & Li, L. (2018). Three-dimensional bioprinting of oppositely charged hydrogels with super strong interface bonding. ACS applied materials & interfaces, 10(13), 11164-11174.

[21] Wang, Q. S., Han, G. C., Yan, S. Q., You, R. C., & Zhang, Q. (2020). Facile Preparation of Silk Fibroin Scaffold Via Direct Solvent Exchange. Journal of Fiber Bioengineering and Informatics, 13(1), 13-21.

[21] Ukpai, G., & Rubinsky, B. (2020). A three-dimensional model for analysis and control of phase change phenomena during 3D printing of biological tissue. Bioprinting, 18. https://doi.org/10.1016/j.bprint.2020.e00077

[22] Ukpai, G., Sahyoun, J., Stuart, R., Wang, S., Xiao, Z., & Rubinsky, B. (2019). A parallel multiple layer cryolithography device for the manufacture of biological material for tissue engineering. Journal of Medical Devices, Transactions of the ASME, 13(3).

[23] Tan, Z., Parisi, C., Silvio, L. Di, Dini, D., & Forte, A. E. (n.d.). Cryogenic 3D Printing of Super Soft Hydrogels. https://doi.org/10.1038/s41598-017-16668-9

[24] Daly, A. C., Critchley, S. E., Rencsok, E. M., & Kelly, D. J. (2016). A comparison of different bioinks for 3D bioprinting of fibrocartilage and hyaline cartilage. Biofabrication, 8(4), 045002.

[25] Kelly, B. E., Bhattacharya, I., Heidari, H., Shusteff, M., Spadaccini, C. M., & Taylor, H. K. (2019). Volumetric additive manufacturing via tomographic reconstruction. Science, 363(6431), 1075-1079.

[26] Na, K., Shin, S., Lee, H., Shin, D., Baek, J., Kwak, H., ... & Hyun, J. (2018). Effect of solution viscosity on retardation of cell sedimentation in DLP 3D printing of gelatin methacrylate/silk fibroin bioink. Journal of Industrial and Engineering Chemistry, 61, 340-347.

[27] Zhou, M., Lee, B. H., & Tan, L. P. (2017). A dual crosslinking strategy to tailor rheological properties of gelatin methacryloyl.

[28] Shi, Y., Xing, T. L., Zhang, H. B., Yin, R. X., Yang, S. M., Wei, J., & Zhang, W. J. (2018). Tyrosinase-doped bioink for 3D bioprinting of living skin constructs. Biomedical Materials, 13(3), 035008.

[29] Costa, J. B., Silva-Correia, J., Oliveira, J. M., & Reis, R. L. (2017). Fast setting silk fibroin bioink for bioprinting of patient-specific memory-shape implants. Advanced Healthcare Materials, 6(22), 1701021.

[30] Peng, W., Datta, P., Ayan, B., Ozbolat, V., Sosnoski, D., & Ozbolat, I. T. (2017). 3D bioprinting for drug discovery and development in pharmaceutics. Acta biomaterialia, 57, 26-46.

[31] Zhao, Y., Yao, R., Ouyang, L., Ding, H., Zhang, T., Zhang, K., ... & Sun, W. (2014). Three-dimensional printing of Hela cells for cervical tumor model in vitro. *Biofabrication*, *6*(3), 035001.

[32] Rodríguez-Dévora, J. I., Zhang, B., Reyna, D., Shi, Z. D., & Xu, T. (2012). High throughput miniature drug-screening platform using bioprinting technology. *Biofabrication*, *4*(3), 035001.

[33] Xu, F., Celli, J., Rizvi, I., Moon, S., Hasan, T., & Demirci, U. (2011). A three-dimensional in vitro ovarian cancer coculture model using a high-throughput cell patterning platform. *Biotechnology journal*, *6*(2), 204-212.

[34] Chang, R., Emami, K., Wu, H., & Sun, W. (2010). Biofabrication of a three-dimensional liver micro-organ as an in vitro drug metabolism model. *Biofabrication*, *2*(4), 045004.

[35] Arutyunyan, I., Elchaninov, A., Sukhikh, G., & Fatkhudinov, T. (2021). Cryopreservation of tissue-engineered scaffold-based constructs: from concept to reality. Stem Cell Reviews and Reports, 1-19.

[36] Shajib, M. S., Futrega, K., Davies, A. M., Franco, R. A. G., McKenna, E., Guillesser, B., ... & Doran, M. R. (2023). A tumour-spheroid manufacturing and cryopreservation process that yields a highly reproducible product ready for direct use in drug screening assays. Journal of the Royal Society Interface, 20(207), 20230468.

[37] Ravanbakhsh, H., & Zhang, Y. S. (2022). Cryobioprinting for biomedical applications. Journal of 3D printing in medicine, 6(4), 163-166.

[38] Bissoyi, A., Nayak, B., Pramanik, K., & Sarangi, S. K. (2014). Targeting cryopreservation-induced cell death: a review. Biopreservation and biobanking, 12(1), 23-34.

[39] Gao, D., & Critser, J. K. (2000). Mechanisms of cryoinjury in living cells. ILAR journal, 41(4), 187-196.

[40] Fujita, J. (1999). Cold shock response in mammalian cells. *J Mol Microbiol Biotechnol*, *1*(2), 243-255.

[41] Mazur, P., Leibo, S. P., & Chu, E. H. (1972). A two-factor hypothesis of freezing injury: evidence from Chinese hamster tissue-culture cells. *Experimental cell research*, *71*(2), 345-355.

[42] Handbook, E. C. A. C. C. (2011). Fundamental Techniques in Cell Culture Laboratory Handbook. *The European Collection of Cell Cultures.[ONLINE] Available at: http://www. sigmaaldrich. com/life-science/cellculture/learning-center/ecacc-handbook. html.[Accessed 09 July 2014]*.

[43] Adamkiewicz, M., & Rubinsky, B. (2015). Cryogenic 3D printing for tissue engineering. Cryobiology. https://doi.org/10.1016/j.cryobiol.2015.10.152

[44] Warburton, L., Liu, C., Dharmadhikari, K., Vemulakonda, P., Cheema, Y., Kewelramani, N., and Sidelnikov, D.,et al 2019, "Utilization of Cryogenic Temperatures to Reduce Line Width Variability in 3D Bioprinted Hydrogel Lattices," Trans. Addit. Manuf. Meets Med., 1(1), epub

[45] Lee, J.; Kim, G. A cryopreservable cell-laden GelMa-based scaffold fabricated using a 3D printing process supplemented with an in situ photo-crosslinking. J. Ind. Eng. Chem. 2020, 85, 249–257.

[46] Luo, Z.; Tang, G.; Ravanbakhsh, H.; Li, W.; Wang, M.; Kuang, X.; Garciamendez-Mijares, C.E.; Lian, L.; Yi, S.; Liao, J.; et al. Vertical extrusion cryo (bio) printing for anisotropic tissue manufacturing. Adv. Mater. 2022, 34, 2108931.

[47] Ravanbakhsh H, Luo Z, Zhang X, Maharjan S, Mirkarimi HS, Tang G, Chávez-Madero C, Mongeau L, Zhang YS. Freeform cell-laden cryobioprinting for shelf-ready tissue fabrication and storage. Matter. 2022 Feb 2;5(2):573-93.

[48] Warburton, L., & Rubinsky, B. (2022). Freezing-modulated-crosslinking: A crosslinking approach for 3D cryoprinting. Bioprinting, 27, e00225.

[49] Freyman, T. M., Yannas, I. V., & Gibson, L. J., 2001, "Cellular materials as porous scaffolds for tissue engineering," Progress in Materials Science, 46(3–4), 273–282.

[50] Feng, P., Wei, P., Shuai, C., & Peng, S., 2014, "Characterization of Mechanical and Biological Properties of 3-D Scaffolds Reinforced with Zinc Oxide for Bone Tissue Engineering" PLoS ONE

[51] Maleki, H., Shahbazi, M. A., Montes, S., Hosseini, S. H., Eskandari, M. R., Zaunschirm, S., Verwanger, T., Mathur, S., Milow, B., Krammer, B., & Hüsing, N., 2019, "Mechanically Strong Silica-Silk Fibroin Bioaerogel: A Hybrid Scaffold with Ordered Honeycomb Micromorphology and Multiscale Porosity for Bone Regeneration," ACS Applied Materials and Interfaces, 11(19), 17256–17269.

[52] De France, K. J., Xu, F., & Hoare, T., 2018, "Structured Macroporous Hydrogels: Progress, Challenges, and Opportunities," Advanced Healthcare Materials, 7(1), 1–17.

[53] Preciado, J. A., Cohen, S., Skandakumaran, P., & Rubinsky, B., 2003, "Utilization of directional freezing for the construction of tissue engineering scaffolds," American Society of Mechanical Engineers, Heat Transfer Division,, Publication) HTD, 374(4), 439–442.

[54] Zhang, Y., Wang, C., Fu, L., Ye, S., Wang, M., & Zhou, Y., 2019, "Fabrication and application of novel porous scaffold in situ-loaded graphene oxide and osteogenic peptide by cryogenic 3D printing for repairing critical-sized bone defect," Molecules, 24(9,

[55] Gutiérrez, M. C., Ferrer, M. L., & del Monte, F., 2008, "Ice-templated materials: Sophisticated structures exhibiting enhanced functionalities obtained after unidirectional freezing and ice-segregation-induced self-assembly," Chemistry of Materials, 20(3), 634-648.

[56] Nishihara, H., Mukai, S. R., Yamashita, D., & Tamon, H., 2005, "Ordered macroporous silica by ice templating," Chemistry of Materials, 17(3), 683–689.

[57] Song, X., Tetik, H., Jirakittsonthon, T., Parandoush, P., Yang, G., Lee, D., Ryu, S., Lei, S., Weiss, M. L., & Lin, D., 2019, "Biomimetic 3D Printing of Hierarchical and Interconnected Porous Hydroxyapatite Structures with High Mechanical Strength for Bone Cell Culture," Advanced Engineering Materials, 21(1), 1–6.

[58] Bozkurt, A., Brook, G. A., Moellers, S., Lassner, F., Sellhaus, B., Weis, J., Woeltje, M., Tank, J., Beckmann, C., Fuchs, P., Damink, L. O., Schügner, F., Heschel, I., & Pallua, N., 2007, "In vitro assessment of axonal growth using dorsal root ganglia explants in a novel three-dimensional collagen matrix," Tissue Engineering, 13(12), 2971–2979.

[59] Qi, X., Ye, J., & Wang, Y., 2009, "Alginate/poly, lactic-co-glycolic acid)/calcium phosphate cement scaffold with oriented pore structure for bone tissue engineering," Journal of Biomedical Materials Research - Part A, 89(4), 980–987.

[60] Kaczmarek-Pawelska, A., 2020, "Alginate-Based Hydrogels in Regenerative Medicine," Alginates - Recent Uses of This Natural Polymer.

[62] Axpe, E., & Oyen, M. L. (2016). Applications of alginate-based bioinks in 3D bioprinting. *International journal of molecular sciences*, *17*(12), 1976.

[63] Tetik, H., Wang, Y., Sun, X., Cao, D., Shah, N., Zhu, H., Qian, F., & Lin, D., 2021, "Additive Manufacturing of 3D Aerogels and Porous Scaffolds: A Review," Advanced Functional Materials, 2103410, 2103410.

[64] Yang, L., Tanabe, K., Miura, T., Yoshinari, M., Takemoto, S., Shintani, S., & Kasahara, M., 2017, "Influence of lyophilization factors and gelatin concentration on pore structures of atelocollagen/gelatin sponge biomaterial," Dental materials journal, 36(4), 429-437.

[65] Shahbazi, M. A., Ghalkhani, M., & Maleki, H., 2020, "Directional Freeze-Casting: A Bioinspired Method to Assemble Multifunctional Aligned Porous Structures for Advanced Applications," Advanced Engineering Materials, 22(7), 2000033.

[66] Annabi, N., Nichol, J. W., Zhong, X., Ji, C., Koshy, S., Khademhosseini, A., & Dehghani, F., 2010, "Controlling the porosity and microarchitecture of hydrogels for tissue engineering," Tissue Engineering - Part B: Reviews, 16(4), 371–383.

[67] Wang, C., Ye, X., Zhao, Y., Bai, L., He, Z., Tong, Q., ... & Wang, M., 2020, " Cryogenic 3D printing of porous scaffolds for in situ delivery of 2D black phosphorus nanosheets, doxorubicin hydrochloride and osteogenic peptide for treating tumor resection-induced bone defects," Biofabrication, 12(3), 035004.

[68] Kim, G., Ahn, S., Yoon, H., Kim, Y., & Chun, W., 2009, "A cryogenic direct-plotting system for fabrication of 3D collagen scaffolds for tissue engineering," Journal of Materials Chemistry, 19(46), 8817–8823.

[69] Liu, H., Zhang, G., & Li, H., 2017, "Preparation and properties of GO-PVA composite hydrogel with oriented structure," In AIP Conference Proceedings, Vol. 1820, No. 1, p. 030009, AIP Publishing LLC.

[70] Fu, S., Thacker, A., Sperger, D. M., Boni, R. L., Buckner, I. S., Velankar, S., Munson, E. J., & Block, L. H., 2011, "Relevance of rheological properties of sodium alginate in solution to calcium alginate gel properties," AAPS PharmSciTech, 12(2), 453–460.

[71] Sahoo, D. R., & Biswal, T., 2021, "Alginate and its application to tissue engineering," SN Applied Sciences, 3(1), 1–19.

[72] Kuo, C. K., & Ma, P. X., 2008, "Maintaining dimensions and mechanical properties of ionically crosslinked alginate hydrogel scaffolds in vitro," Journal of Biomedical Materials Research - Part A, 84(4), 899–907.

[73] Hurler, J., Engesland, A., Poorahmary Kermany, B., & Škalko-Basnet, N., 2012, "Improved texture analysis for hydrogel characterization: Gel cohesiveness, adhesiveness, and hardness," Journal of Applied Polymer Science, 125(1), 180-188.

[74] Remaggi, G., Catanzano, O., Quaglia, F., & Elviri, L. (2022). Alginate Self-Crosslinking Ink for 3D Extrusion-Based Cryoprinting and Application for Epirubicin-HCl Delivery on MCF-7 Cells.

[75] Warburton, L., Lou, L., & Rubinsky, B. (2022). A Modular Three-Dimensional Bioprinter for Printing Porous Scaffolds for Tissue Engineering. Journal of Heat Transfer, 144(3), 031205.

[76] Dar, A., Shachar, M., Leor, J., & Cohen, S. (2002). Optimization of cardiac cell seeding and distribution in 3D porous alginate scaffolds. Biotechnology and bioengineering, 80(3), 305-312.

[77] Hecht, H., & Srebnik, S. (2016). Structural Characterization of Sodium Alginate and Calcium Alginate. Biomacromolecules, 17(6), 2160–2167. https://doi.org/10.1021/acs.biomac.6b00378

[78] Lee, K. Y., & Mooney, D. J. (2012). Alginate: Properties and biomedical applications. Progress in Polymer Science (Oxford), 37(1), 106–126. https://doi.org/10.1016/j.progpolymsci.2011.06.003

[79] Skjak-Braek G, Grasdalen H, Smidsrod O (1989) Inhomogeneous Polysaccharide Ionic Gels. Carbohydr Polym 10:31–54.

[80] Kim H-S (1990) A kinetic study on calcium alginate bead formation. Korean J Chem Eng 7(1):1–6.

[81] Mikkelsen A, Elgsaeter A (1995) Density distribution of calcium-induced alginate gels. A numerical study. Biopolymers 36(1):17–41.

[82] Duez J-M, et al. (2000) NMR studies of calcium induced alginate gelation. PartI - MRI tests of gelation models. Magn Reson Chem 38:324–330.

[83] Hajikhani A, Wriggers P, Marino M (2021) Chemo-mechanical modelling of swelling and crosslinking reaction kietics in alginate hydrogels: A novel theory and its numerical implementation. J Mech Phys Solid 153:104476.

[84] Braschler, T., Valero, A., Collela, L., Pataky, K. Brugger, J. Renauld P (2011) Link between alginate reaction front propagation and general reaction diffusion theory. Anal Chem 83:2234–2242.

[85] Carslaw HS, Jaeger JC (1959) Conduction of Heat in Solids (Clarendon Press, Oxford, England, UK). Second Edi.

[86] Rubinsky B, Cravalho EG (1979) The determination of the thermal history in a one-dimensional freezing system by a perturbation method. J Heat Transfer 101(2):326–330.

[87] Hazur, J., Detsch, R., Karakaya, E., Kaschta, J., Teßmar, J., Schneidereit, D., ... & Boccaccini, A. R. (2020). Improving alginate printability for biofabrication: Establishment of a universal and homogeneous pre-crosslinking technique. Biofabrication, 12(4), 045004.

[88] Łabowska, M. B., Jankowska, A. M., Michalak, I., & Detyna, J. (2021). Shrinkage of Alginate Hydrogel Bioinks Potentially Used in 3D Bioprinting Technology. In Key Engineering Materials (Vol. 885, pp. 39-45). Trans Tech Publications Ltd.

[89] Feng, P., Wei, P., Shuai, C., & Peng, S., 2014, “Characterization of Mechanical and Biological Properties of 3-D Scaffolds Reinforced with Zinc Oxide for Bone Tissue Engineering” PLoS ONE, 9(1,

[90] Maleki, H., Shahbazi, M. A., Montes, S., Hosseini, S. H., Eskandari, M. R., Zaunschirm, S., Verwanger, T., Mathur, S., Milow, B., Krammer, B., & Hüsing, N., 2019, “Mechanically Strong Silica-Silk Fibroin Bioaerogel: A Hybrid Scaffold with Ordered Honeycomb Micromorphology and Multiscale Porosity for Bone Regeneration,” ACS Applied Materials and Interfaces, 11(19), 17256–17269.

[91] Tetik, H., Wang, Y., Sun, X., Cao, D., Shah, N., Zhu, H., Qian, F., & Lin, D., 2021, “Additive Manufacturing of 3D Aerogels and Porous Scaffolds: A Review,” Advanced Functional Materials, 2103410, 2103410.

[92] Kiesslich, S., & Kamen, A. A. (2020). Vero cell upstream bioprocess development for the production of viral vectors and vaccines. Biotechnology advances, 44, 107608.

[93] Zhang, C., Zhou, Y., Zhang, L., Wu, L., Chen, Y., Xie, D., & Chen, W. (2018). Hydrogel cryopreservation system: an effective method for cell storage. International journal of molecular sciences, 19(11), 3330.

[94] Stacey, G. N., & Masters, J. R. (2008). Cryopreservation and banking of mammalian cell lines. Nature protocols, 3(12), 1981-1989.

[95] Mazur, P. (1984). Freezing of living cells: mechanisms and implications. American journal of physiology-cell physiology, 247(3), C125-C142.

[96] Stacey, G. N., & Masters, J. R. (2008). Cryopreservation and banking of mammalian cell lines. Nature protocols, 3(12), 1981-1989.

[97] Rahana, A. R., Ng, S. P., Leong, C. F., & Rahimah, M. D. (2011). Comparison between mechanical freezer and conventional freezing using liquid nitrogen in normozoospermia. Singapore medical journal, 52(10), 734. Comparison to cryopreservation in liquid nitrogen. Materia Medica Polona. Polish Journal of Medicine and Pharmacy, 26(2), 69-72.

[98] Ratajczak, M. Z., Kregenow, D. A., Kuczyński, W. I., Ratajczak, J., & Gewirtz, A. M. (1994). The storage of cells from different tumor lines in a mechanical freezer at-80 degrees C.

[99] McGann, L. E., & Farrant, J. (1976). Survival of tissue culture cells frozen by a two-step procedure to− 196° CI Holding temperature and time. Cryobiology, 13(3), 261-268.

[100] Higgins, A. Z., Cullen, D. K., LaPlaca, M. C., & Karlsson, J. O. (2011). Effects of freezing profile parameters on the survival of cryopreserved rat embryonic neural cells. Journal of neuroscience methods, 201(1), 9-16.

[101] Nsabimana, E., Kisidayova, S., Macheboeuf, D., Newbold, C. J., & Jouany, J. P. (2003). Two-step freezing procedure for cryopreservation of rumen ciliates, an effective tool for creation of a frozen rumen protozoa bank. Applied and environmental microbiology, 69(7), 3826-3832.

[102] Blaeser, A., Duarte Campos, D. F., Puster, U., Richtering, W., Stevens, M. M., & Fischer, H. (2016). Controlling shear stress in 3D bioprinting is a key factor to balance printing resolution and stem cell integrity. Advanced healthcare materials, 5(3), 326-333.

[103] Baust, J. M., Snyder, K. K., Van Buskirk, R. G., & Baust, J. G. (2022). Assessment of the impact of post-thaw stress pathway modulation on cell recovery following cryopreservation in a hematopoietic progenitor cell model. Cells, 11(2), 278.

[104] Rauen, U., Polzar, B., Stephan, H., Mannherz, H. G., & De Groot, H. E. R. B. E. R. T. (1999). Cold-induced apoptosis in cultured hepatocytes and liver endothelial cells: mediation by reactive oxygen species. The FASEB Journal, 13(1), 155-168.

[105] Warburton, L., & Rubinsky, B. (2023). Cryopreservation of 3D Bioprinted Scaffolds with Temperature-Controlled-Cryoprinting. *Gels*, *9*(6), 502.

[106] Rabin, R. C. (2022). Doctors transplant ear of human cells, made by 3-D printer. *The New York Times*, *2*.

[107] Zhao et al., (2023). In vivo bioprinting: Broadening the therapeutic horizon for tissue injuries. Bioactive Materials, 25, 201-222.

[108] Tomás, R. M., Bissoyi, A., Congdon, T. R., & Gibson, M. I. (2022). Assay-ready cryopreserved cell monolayers enabled by macromolecular cryoprotectants. *Biomacromolecules*, *23*(9), 3948-3959.

[109] Ma, L., Wu, Y., Li, Y., Aazmi, A., Zhou, H., Zhang, B., & Yang, H. (2020). Current advances on 3D-bioprinted liver tissue models. *Advanced healthcare materials*, *9*(24), 2001517